Chemical Science

ROYAL SOCIETY OF CHEMISTRY

REVIEW

View Article Online
View Journal | View Issue

Cite this: *Chem. Sci.*, 2021, **12**, 8967

Directing transition metal-based oxygen-functionalization catalysis

Gracita M. Tomboc, Yeji Park, Kwangyeol Lee * and Kyoungsuk Jin *

This review presents the recent progress of oxygen functionalization reactions based on non-electrochemical (conventional organic synthesis) and electrochemical methods. Although both methods have their advantages and limitations, the former approach has been used to synthesize a broader range of organic substances as the latter is limited by several factors, such as poor selectivity and high energy cost. However, because electrochemical methods can replace harmful terminal oxidizers with external voltage, organic electrosynthesis has emerged as greener and more eco-friendly compared to conventional organic synthesis. The progress of electrochemical methods toward oxygen functionalization is presented by an in-depth discussion of different types of electrically driven-chemical organic synthesis, with particular attention to recently developed electrochemical systems and catalyst designs. We hope to direct the attention of readers to the latest breakthroughs of traditional oxygen functionalization reactions and to the potential of electrochemistry for the transformation of organic substrates to useful end products.

Received 4th March 2021
Accepted 7th June 2021

DOI: 10.1039/d1sc01272j

rsc.li/chemical-science

1. Introduction

Oxygen atom functionalization has played an indispensable role in industrial applications and biological processes. For example, epoxides are versatile chemical intermediates that have been mainly produced from the oxygen functionalization of olefin substrates. Indeed, ethylene oxide and propylene oxide are among the highest volume products in our industry, with annual production rates of 15 and 3 Mt per year, respectively. These epoxides are widely used to manufacture diverse products, including ethylene glycol, ethylene carbonate, polyester, polyethylene glycol, and polyurethane. Representative examples of oxygen functionalization other than epoxidation are C–H bond oxidation, sulfoxidation, phosphorous oxidation, allylic oxidation, lactonization, Baeyer–Villiger oxidation, *etc.*

In nature, there exist various enzymes that are capable of oxidizing target substrates with high selectivity. For example, methane monooxidase (MMO) in methanotrophic bacteria

Department of Chemistry and Research Institute for Natural Sciences, Korea University, Seoul 02841, Republic of Korea. E-mail: kylee1@korea.ac.kr; kysjin@korea.ac.kr

Dr Gracita M. Tomboc received her Bachelor's degree in Chemical Engineering from Adamson University, Manila Philippines in 2012. She became a registered Chemical Engineer in 2013. She received her PhD degree in Energy Science and Technology from Myongji University, Republic of Korea in 2019. She is currently working as post-doctoral researcher at Korea University. Her research interests include the advanced materials processing of ideal electrode materials for electrochemical energy storage system applications such as supercapacitor, water splitting process, direct methanol fuel cells, and hydrogen generation.

Professor Kwangyeol Lee obtained his PhD degree (1997) in Chemistry from the University of Illinois at Urbana-Champaign. After fulfilling his military obligation, he joined Korea University in 2003 as a chemistry faculty member, before being appointed as a professor. He is the recipient of the Wiley-KCS Young Scholar Award (2009, Korean Chemical Society) and the Excellent Research Award (2019, KCS Inorganic Chemistry Division). His current interests include the development of synthetic methodologies for nanoscale materials and the development of nanotechnologies to support the environment by creating sustainable energy.

oxidizes methane into methanol under ambient conditions.[1,2] Interestingly, the active site of the MMO enzyme is comprised of copper-based particulate MMO (pMMO) and iron-based soluble MMO (sMMO) that selectively capture the methane substrate.[3] In addition to MMO, several transition metal-based enzymes are known to catalyze several oxygen functionalization reactions.[4,5] Inspired by nature, various synthetic transition metal-based complexes have been investigated to mimic biological systems.[6,7] In line with this, oxygen-atom functionalization generally follows the stepwise process shown below:

$$M^{x}O_{y}L + \text{oxidant} \rightarrow M^{x+2}O_{y+1}L$$

$$M^{x+2}O_{y+1}L + \text{subs} \rightarrow M^{x}O_{y}L + \text{prods},$$

where M is the transition metal ion, O_yL is the ligand molecule coordinated to the central metal ion, subs is the target substrates, and prods is the oxidized products. The addition of chemical oxidant first activates the catalysts ($M^{x}O_{y}L$) to make oxidized intermediate species ($M^{x+2}O_{y+1}L$). The unstable intermediates with high oxidizing power subsequently provide oxygen to the substrate to generate final products. Investigation of an efficient metal complex catalyst (or heterogeneous catalyst) and its counter chemical oxidant for various oxygen functionalization reactions have been widely studied. Currently, industrially relevant oxygen functionalization is being pursued as a non-electrochemical method with heterogeneous catalysts (see Section 2.3.3).

Apart from this route, an oxygen-functionalization reaction can be conducted *via* electrochemical methods, where an external voltage is applied to drive the reaction instead of oxidants. Although relatively low catalytic performance and limited reaction scope have been reported compared to the one by the non-electrochemical pathways, it has been regarded as a promising alternative as electrification itself does not require any additives and is ideally free of greenhouse gas (GHG, CO/CO_2) emission.

Professor Kyoungsuk Jin is an assistant professor in the department of chemistry at Korea University. He received his PhD degree (2016) in Material Science from Seoul National University. During his postdoctoral research at the Massachusetts Institute of Technology (MIT), he studied the electrochemical oxygen functionalization reactions. He joined the department of chemistry at Korea University to begin his independent career in 2020. His research focuses on the fundamental understanding of electrochemical reactions and organic electrosynthesis including various oxygen-atom functionalization catalysis, asymmetric synthesis, biochemical reactions.

This review aims to provide an overview of previous oxygen functionalization studies, which are divided into two parts: non-electrochemical and electrochemical methods. We categorized non-electrochemical methods according to their synthetic routes, namely, chemical route, photochemical route, and heterogeneous catalysis. We also discussed various catalytic systems, focusing on reaction mechanism, high-valent metal–oxo complexes, heterogeneous catalysts, and oxidants. The second part of this work featured recent studies and research directions of electrochemical oxygen functionalization. We divided electrochemical oxygen functionalization into three groups: (1) direct oxidation *via* outer-sphere electron transfer, (2) indirect oxidation, and (3) direct oxidation *via* inner-sphere electron transfer. In addition, recent progress in electrochemical oxygen functionalization was classified according to their synthetic strategies and interfacial kinetics. Lastly, the future direction of electrochemical oxygen functionalization will be described based on current understanding.

2. Non-electrochemical oxygen functionalization

For many years, oxidative reaction mostly followed stoichiometric oxidations, which consume toxic and corrosive organic reagents with high oxidizing capacity, such as bromine (Br_2),[8] chromium trioxide (CrO_3),[9] and potassium permanganate ($KMnO_4$).[10] This process could cause severe damage to the environment associated with the production of vast amounts of heavy-metal waste. As a result, many new works leaned towards the development of greener catalytic oxidations catalyzed by various metals and metal complex catalysts under mild conditions. The progress of catalytic processes directs the exploration of oxidants that give no waste as by-products and the use of inexpensive catalysts that are easy to prepare, handle, regenerate, and are stable and reactive under mild reaction conditions.[11,12]

The oxidation of organic molecules primarily represents either the elimination of hydrogen, as in the sequential dehydrogenations of ethane: $CH_3CH_3 \rightarrow CH_2{=}CH_2 \rightarrow HC{\equiv}CH$, or the replacement of a hydrogen atom bonded to carbon with a more electronegative element like oxygen, as in the series of oxidative transformations of methane: $CH_4 \rightarrow CH_3OH \rightarrow CH_2O \rightarrow HCO_2H \rightarrow CO_2$.[13] Selective oxidation reactions of alcohols, alkanes, and alkenes are some of the most important transformations in chemical synthesis that directly produce essential chemicals and intermediates, such as aldehydes, acids, alcohols, epoxides, and ketones.[14] Here, we categorize non-electrochemical oxygen functionalization according to its synthetic routes and highlight the reaction mechanisms, generation of high-valent metal oxo species, and different catalysts and chemical oxidants typically considered for the oxidative transformation of organic substrates.

2.1. Oxygen atom sources

Chemical oxidants play an important role in the formation of metal–oxo complexes as they function as both an oxygen source

and activating catalysts in oxygen functionalization.[15] Molecular O_2, hydrogen peroxide (H_2O_2), potassium bisulfate ($KHSO_4$), chromate (CrO_4), sodium hypochlorite (NaOCl), *tert*-butyl hydroperoxide (TBHP), iodosylbenzene (PhIO), and peroxyacid (RCO_3H) have been widely employed to assist the formation of metal–oxo species under various reaction conditions.[16] Among these, molecular O_2 has been broadly investigated since it is abundant, cheap, and only produces water as a by-product.[17] The activation of molecular O_2 on the surface of heterogeneous catalysts is the key step in different oxidation reactions, such as epoxidation and CO-, hydrocarbon-, alcohol-, and glucose-oxidations.[18] However, oxidation reactions using molecular O_2 oxidant often have several challenges: (1) the direct oxidation of organic substrates using molecular O_2 typically occurs at harsh conditions (toxic solvents, high temperature, and high pressure); (2) a co-reductant is normally required to complete the oxidation of transition metal-based catalysis; and (3) product selectivity is relatively moderate.[18,19] Likewise, hydrogen peroxide has been studied as it also generates water as its by-product. Fe-, Mn-, Rh-, W-, and Ti-based catalytic systems are known for employing H_2O_2 as the terminal oxidant.[20–24] The major limitations of this oxidant are the hazards associated with the storage and transportation of H_2O_2 and the requirement of toxic organic solvents for the recovery of catalysts used during its production.[14,25,26]

On the other hand, water is perhaps the most environmentally benign oxygen source for different organic oxidation reactions. However, the problem of using water for organic oxidations is correlated to its stoichiometric catalytic activation. The reaction usually requires strong oxidants, like Ce^{IV} and ammonium nitrate, to remove electrons and protons. *e.g.* $RH + H_2O \xrightarrow{\text{catalyst}} ROH + 2e^- + 2H^+$.[27–30] In line with this, Nam *et al.* recently suggested that much weaker oxidants can replace these strong one-electron oxidants if the reaction is light-driven (see Section 2.2 for details).[6,30,31]

2.2. Metal–oxo species

High-valent metal oxo species, M^{n+}=O or M^{n+}–OH, are highly reactive intermediates that are widely utilized in various oxidation processes in biological systems and chemical industries. In enzymatic and synthetic oxidation catalysis, high-valent transition metal–oxo intermediates are generally produced and serve as the active oxygen atom transfer (OAT) species. Transition metal-based high-valent metal–oxo complexes, such as Fe-, Mn-, Ru-, Cr-, Mo-, V-, and Os–oxo complexes, have been investigated.[32–35] The oxidizing power of the high-valent oxo-form of these metal atoms is sufficient for the oxidation of target substrates. The structures, properties, and reactivities of these complexes in organic oxidation reactions have been well documented in the past.[7,36] Fig. 1 presents some of the representative metal–oxo species employed for oxygen functionalization reactions, including Fe-, Mn-, and Ru–oxo complexes.

Oxidation reactions such as alkane hydroxylation, olefin epoxidation, and olefin *cis*-dihydroxylation catalyzed by iron centers in enzymes have been a subject of interest for many years. High-valent porphyrin Fe–oxo intermediates are central oxidizing species in heme and non-heme iron enzymes and synthetic oxidation catalysts.[37–41] Fig. 1a displays the examples of synthetic model systems of high-valent Fe–oxo porphyrin complex. Among these, Fe^{IV}–oxo porphyrin π-cation radical

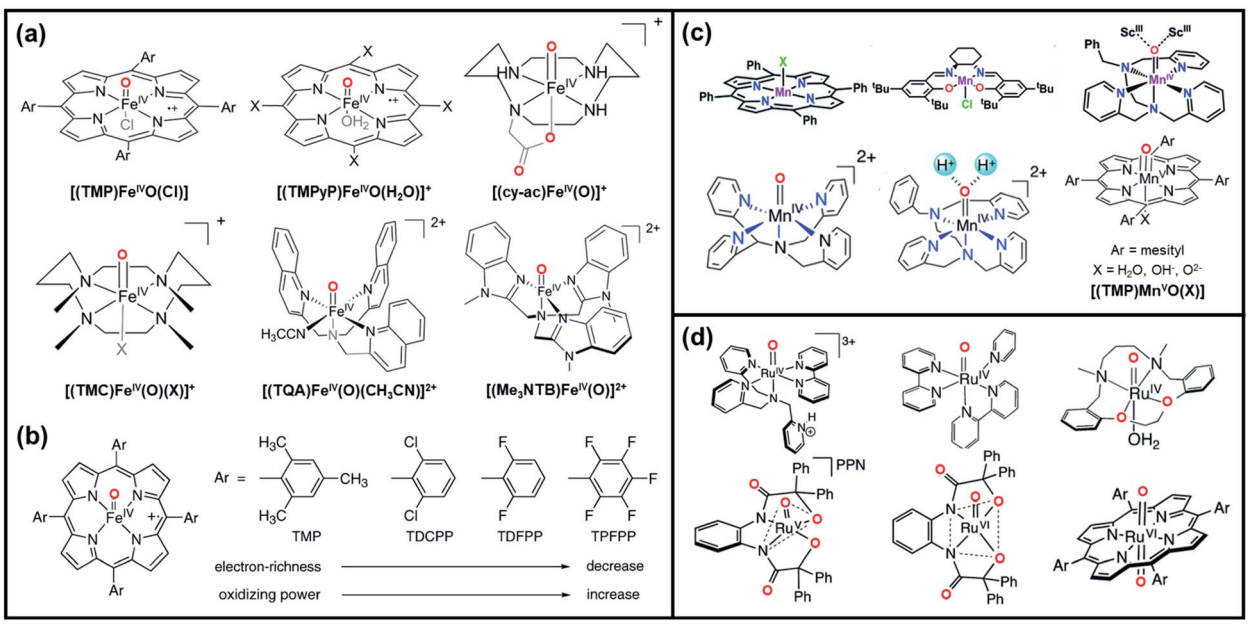

Fig. 1 (a) Examples of high-valent Fe–oxo porphyrin complex. Reproduced with permission.[33] Copyright 2018, American Chemical Society. (b) Correlation between Fe^{IV}–oxo species paired with different axial ligands and their reactivities. Reproduced with permission.[193] Copyright 2007, American Chemical Society. (c) Representatives of high-valent Mn–oxo porphyrin and salen complex. Reproduced with permission.[33,53,194] Copyright 2020, The Royal Society of Chemistry; Copyright 2016, American Chemical Society; and Copyright 2018, American Chemical Society. (d) Examples of high-valent Ru–oxo porphyrin complex. Reproduced with permission.[54] Copyright 2016, The Royal Society of Chemistry.

$[(P^{\bullet+})Fe^{IV}(O)]$ is a well-known intermediate formed during the reaction of Fe(TMP)Cl (TMP = *meso*-tetramesitylporphyrin) and *m*-chlorobenzoic acid (*m*-CPBA) in presence of dichloromethane and methanol. The formed Fe–oxo species was found to be a competent oxidant in olefin epoxidation.[4,5,42–45] Likewise, Fe^{IV}–oxo tetraphenylporphyrin $[(TPP)Fe^{IV}(O)]^{\bullet+}$ produced *via* the oxidation of Fe^{III} tetraphenylporphyrin chloride $[(TPP)Fe^{III}(Cl)]$ and PhIO with cytochrome P450 catalyst are discovered as reactive oxo species for driving alkane hydroxylation.[4,5,43,44] Since then, Fe^{IV}–oxo species with electron-rich/deficient porphyrins paired with different axial ligands (Fig. 1b) have been designed and investigated towards various oxidation reactions in an effort to understand the electronic effects of porphyrin and axial ligands on the chemical properties of the Fe–oxo intermediates.[40,41,46]

High-valent Mn–oxo species have also received a great deal of attention for oxygen functionalization reactions. The model complexes of manganese are categorized into two groups based on the ligand systems: (1) Mn–porphyrin based systems and (2) Mn–salen based systems. Groves *et al.* synthesized the three kinds of Mn=O complexes namely, (TMP)Mn(O), (TMP)Mn(O)(OH), and (TPP)Mn(O) (TMP = 5, 10, 15, 20-tetramesitylporphyrin), by facile reaction of Mn^{III} complex with *m*-CPBA as oxidants. The generated transient species were assigned to Mn^{V}=O species, which showed high reactivity towards olefin substrates, thus forming epoxide products.[47] Similarly, high-valent Mn^{IV}–oxo species generated from the oxidation of tetra-*N*-((methylpyridyl)-porphyrinato)Mn^{III}-complex $[Mn^{III}(TMPyP)]$ are identified as active species for olefin epoxidation and alkane hydroxylation catalysis.[37,48–50] Moreover, manganese–salen complexes (Mn–salen) are well-known catalysts in the epoxidation of alkenes and other olefinic materials. Mn–salen complexes with PhIO as terminal oxidant are typically oxidized to Mn^{V}(salen)=O, which are considered as the active species responsible for the epoxidation of various substrates.[51] In particular, the Jacobsen's catalyst, a chiral salen based Mn^{III} complex, successfully transformed wide range of substrates including conjugated *Z*-enynes, acyclic conjugated polyenes, cyclic dienes, enol ethers, and some tetra-substituted conjugated alkenes.[52] The combination of this catalyst with iodosyl benzene and triethylamine trihydrofluoride as fluoride donor showed selective fluorination of a large variety of substrates containing benzylic C–H bond. The representative examples of Mn–oxo species are shown in Fig. 1c.[53]

Lastly, high-valent Ru–oxo species, such as Ru^{IV}=O, Ru^{V}=O, and Ru^{VI}=O, have emerged as reactive species for water oxidation, epoxidation, and C–H oxidation.[54] Ruthenium imine complexes, like $Ru(bpy)_2Cl_2$ (bpy = 2,2′-bipyridine), are among the most distinguished ruthenium complexes oxidized to generate the Ru^{IV}=O intermediate.[55] Interestingly, the catalytic epoxidation efficiency of $Ru(bpy)_2Cl_2$ was increased upon the incorporation of Lewis acid like $Al(OTf)_3$ (OTF: trifluoromethanesulfonate), which led to the formation of more active species, the Ru^{IV}=O/Al^{III} intermediate. Such results have highlighted the roles of non-redox metal ions, like Lewis acids, in regulating the reactivity of high-valent metal–oxo complexes.[56] On the other hand, Ru^{V}–oxo complexes, like $[Ru^{V}(O)(N_4O)^{2+}]$ (N_4O = bis (2-(2-pyridyl)-ethyl)(2-hydroxy-2-(2 pyridyl)ethyl)amine), have been reported to proceed with the oxidative C=C bond cleavage of styrene and *trans*- and *cis*-stilbene in the presence of acetonitrile, leading to the formation of benzaldehyde products. Additionally, *trans*-dioxo-Ru^{VI}–porphyrin complexes $[(Ru^{VI}(TMP)O_2)]$ are well-known intermediates for aerobic asymmetric epoxidation of olefins.[57,58] Fig. 1d displays some examples of high-valent Ru–oxo porphyrin complex.

The details of the electron transfer mechanisms and catalytic performances of metal–oxo species towards various oxygen functionalization reactions are discussed in the succeeding sections.

2.3. Proposed non-electrochemical oxygen functionalization mechanism

In this section, we present the recent progress of non-electrochemical methods for oxygen functionalization. The non-electrochemical methods for the transformation of organic molecules are categorized based on synthetic routes, namely, the (1) chemical route, (2) photochemical route, and (3) heterogeneous catalysis. Scheme 1 displays a schematic illustration of non-electrochemical methods for oxidation functionalization.

An oxygen functionalization reaction *via* chemical route is generally catalyzed by high-valent metal–oxo complexes in presence of chemical oxidants, like H_2O_2 or molecular O_2, under high temperature and pressure. The photochemical route undergoes a similar reaction mechanism as that of the chemical route, except for the utilization of solar radiant energy as the driving force of the organic transformations, which thus enables the oxidation reaction under milder conditions. A typical photochemical oxygen functionalization reaction uses a photosensitizer, chemical oxidant, homogenous catalyst, oxygen source, and substrate. Conversely, oxygen functionalization *via* heterogeneous catalysis proceeds *via* the adsorption of reactant molecules on the catalyst surface, which are converted into surface intermediates, followed by the formation and desorption of the final product. High temperature and pressure are the usual activation conditions of this pathway, while the reaction kinetics are highly dependent on the activation energies (E_a) of adsorbed reactants, adsorbed intermediates, and desorption of products. The activity, selectivity, resistance to deactivation, and regeneration of catalyst are vital properties in heterogeneous catalysis, especially at the industrial level.[22,59,60]

2.3.1. Chemical routes. In the case of Fe-based molecular catalysts, both Fe^{IV}(O)–porphyrin$^{\bullet+}$ and Fe^{V}(O)(OH) reactive intermediates have been proposed to catalyze various kinds of oxygen functionalization reactions.[7,37,61] Although the reactivity profiles for Fe^{V}(O)(OH) are much more limited than the isoelectronic Fe^{IV}(O) porphyrin cation radical species, there have been particular efforts given to understand the involvement of Fe^{V}(O)(OH) during epoxidation of olefins.[62–66] For example, Gupta *et al.* reported the epoxidation mechanism of alkenes using Fe^{V}(O) species derived from biuret-modified Fe–

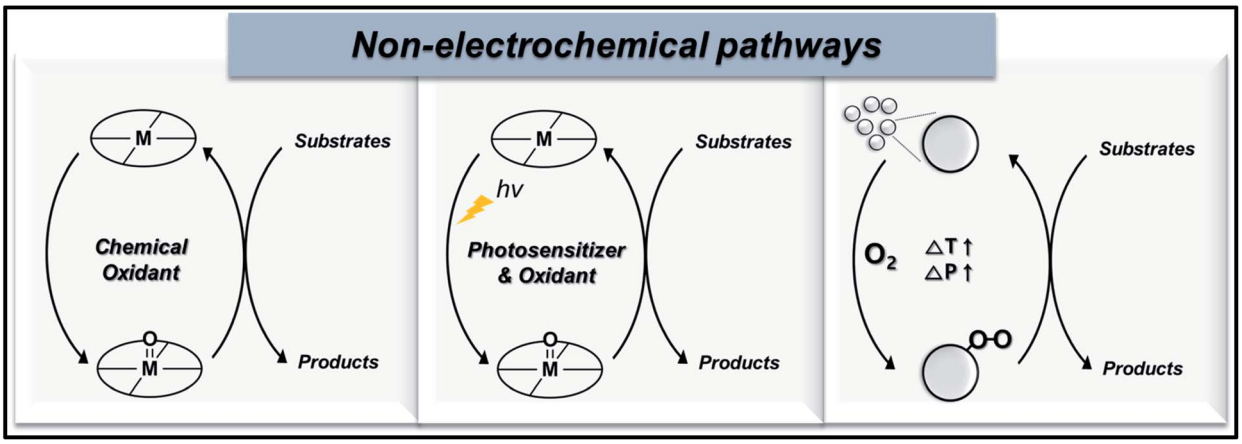

Scheme 1 Schematic illustration of non-electrochemical pathways: (from left to right) chemical route, photochemical route, and heterogeneous catalysis.

TAML complex (tetraamido macrocyclic ligands) at room temperature with NaOCl/*m*-CPBA (*meta*-chloroperoxybenzoic acid) as an oxidant.[67] They proposed three possible pathways of epoxidation, including (1) radical intermediate formation *via* electrophilic attack of $Fe^{V}(O)$ on the alkene associated with C–O bond formation (Fig. 2a, pathway A), (2) generation of the acyclic carbocation radical through one-electron transfer (Fig. 2a, pathway B), and (3) the transfer of oxygen into the alkene by a concerted process (Fig. 2a, pathway C). The combined results of experimental and density functional theory (DFT) calculations have shown that epoxidation using biuret-modified Fe–TAML as catalyst and NaOCl as a chemical oxidant is likely to proceed *via* a two-step process (Fig. 2b). The first step is the generation of a radical intermediate through an electrophilic attack on alkene and the second step is a rapid ring-closing to obtain the epoxide products. The electrophilic character of $Fe^{V}(O)$ species was fully supported by the calculated second-order rate constant (k_2) for the reaction of different alkenes, which revealed an 8000-fold rate difference between electron-rich and electron-deficient substrates. Table 1 (entries 1–9) summarizes the epoxidation of different alkenes by $Fe^{V}(O)$ at room temperature in acetonitrile under air atmosphere. This

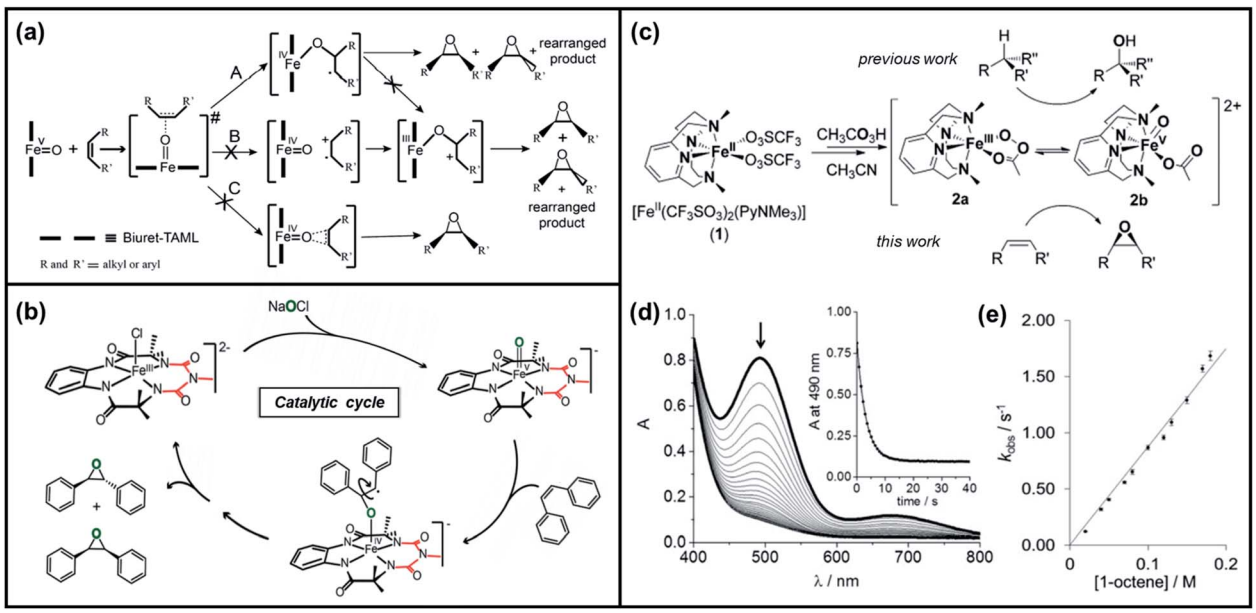

Fig. 2 (a) Three possible mechanisms of epoxidation of alkenes by [$Fe^{V}(O)$–(biuret-TAML)] based on the initial attack of "O" into the substrate during the oxidation reaction and (b) the suggested catalytic cycle for epoxidation of olefins by $Fe^{V}(O)$ and NaOCl. Reproduced with permission.[67] Copyright 2015, American Chemical society. (c) Formation of species **2a** and **2b** upon the reaction of [$Fe^{II}(CF_3SO_3)_2(PyNMe_3)$] with peracetic acid in acetonitrile, (d) kinetics monitoring of the reaction of **2** with 1-octene in acetonitrile/acetone *via* UV/vis spectroscopy (inset displays the decay of the 490 nm chromophore fitted to a single exponential), and (e) plot of rate constants k_{obs} against the 1-octene concentration for the reaction of **2** with 1-octene. Reproduced with permission.[72] Copyright 2016, Wiley-VCH.

Table 1 Catalytic oxidation reactions of different alkenes *via* chemical route catalyzed by $Fe^{V}(O)$ intermediate, Mn^{IV}=O species, and Ru^{IV}=O intermediate with Sc^{3+}, respectively

Entry	Catalyst	Oxidant	Substrate	Product	% yield	% conversion
1	$Fe^{V}(O)$[a]	NaOCl/*m*-CPBA	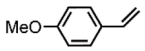	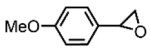	74 ± 6	N.D.
2	$Fe^{V}(O)$[a]	NaOCl/*m*-CPBA		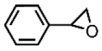	71 ± 6	N.D.
3	$Fe^{V}(O)$[a]	NaOCl/*m*-CPBA	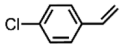	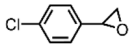	70 ± 6	N.D.
4	$Fe^{V}(O)$[a]	NaOCl/*m*-CPBA	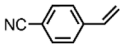	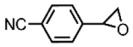	62 ± 5	N.D.
5	$Fe^{V}(O)$[a]	NaOCl/*m*-CPBA	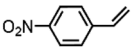	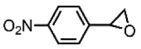	66 ± 5	N.D.
6	$Fe^{V}(O)$[a]	NaOCl/*m*-CPBA	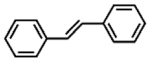	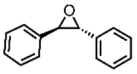	81 ± 4	N.D.
7	$Fe^{V}(O)$[a]	NaOCl/*m*-CPBA			65 ± 5	N.D.
8	$Fe^{V}(O)$[a]	NaOCl/*m*-CPBA	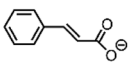	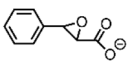	86 ± 6	N.D.
9	$Fe^{V}(O)$[a]	NaOCl/*m*-CPBA			78 ± 7	N.D.
10	$Mn(TPA)Cl_2$[b]	$PhI(OAc)_2$			4.1[c] 91.4[d]	9.9[c] 97.8[d]
11	$Mn(TPA)Cl_2$[b]	$PhI(OAc)_2$			6.7[c] 69.0[d]	9.9[c] 91.3[d]
12	$Mn(TPA)Cl_2$[b]	$PhI(OAc)_2$			5.1[c] 47.4[d]	11.1[c] 84.3[d]
13	$Mn(TPA)Cl_2$[b]	$PhI(OAc)_2$		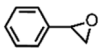	4.9[c] 45.1[d]	9.1[c] 71.9[d]
14	$Mn(TPA)Cl_2$[b]	$PhI(OAc)_2$		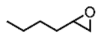	3.7[c] 51.7[d]	9.3[c] 75.1[d]
15	$Mn(TPA)Cl_2$[b]	$PhI(OAc)_2$	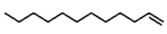	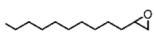	2.5[c] 45.1[d]	13.5[c] 90.3[d]
16	$Ru(bby)_2Cl_2$[e]	$PhI(OAc)_2$			89.9	100
17	$Ru(bby)_2Cl_2$[e]	$PhI(OAc)_2$			82.2	100
18	$Ru(bby)_2Cl_2$[e]	$PhI(OAc)_2$			33.6	98.9
19	$Ru(bby)_2Cl_2$[e]	$PhI(OAc)_2$		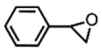	30.0	10
20	$Ru(bby)_2Cl_2$[e]	$PhI(OAc)_2$		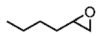	74.6	94.6
21	$Ru(bby)_2Cl_2$[e]	$PhI(OAc)_2$			67.3	100

[a] $[Fe^{V}(O)$–(biuret-TAML)$]^{-}$ complex **2**.[67] [b] $Mn(TPA)Cl_2$ (TPA = tris(pyridin-2-ylmethyl)amine). [c] 1 : 0 ratio Mn^{II} : Al^{3+}. [d] 1 : 0 ratio Mn^{II} : Al^{3+}.[74] [e] $Ru(bpy)_2Cl_2$ (bpy = 2,2′ -bipyridine).[55]

study suggested that Fe^{V}–oxo are more reactive than their analogous Fe^{IV}–oxo species in terms of chemical yield and faradaic efficiency.[68–71]

Costas *et al.* further scrutinized the reactivity of $Fe^{V}(O)$ intermediate for catalytic epoxidation reactions.[72] As shown in Fig. 2c, the reaction of $[Fe^{II}(CF_3SO_3)_2(PyNMe_3)]$ (compound **1**) with peracetic acid and acetonitrile at −41 °C led to the formation of compound **2**, which is made up of two thermally unstable components: $[Fe^{III}(OOAc)(PyNMe_3)]^{2+}$(**2a**) and $[Fe^{V}(O)(OAc)(PyNMe_3)]^{2+}$ (**2b**). The group investigated the reaction kinetics of **2b** with cyclooctene substrate by conducting a series of ultraviolet/visible (UV/vis) stopped-flow experiments.

The rapid disappearance of the absorbance band at 490 nm following the addition of excess olefin was primarily used as an evaluation point (Fig. 2d). Three crucial observations stemmed from these results. First, based on the plot of the rate constant *versus* substrate concentration (Fig. 2e), it was determined that the second-order reaction rates of $Fe^{V}(O)^{+}$ are independent of the peracid concentration. Next, the oxidation rate of **2b** towards olefins was directly proportional to the degree of olefin substitution. Such observation implied that rather than the steric factors, the electronic effects actually dominated the reactivity of the $Fe^{V}(O)$ intermediate towards olefins. Finally, the higher reactivity of 2b compared to synthetic Fe^{IV}–oxo porphyrin radical species supported the proposal of $Fe^{V}(O)$ intermediates as plausible oxygen functionalization agents for high selective epoxidations.

Moreover, the catalytic oxidation of various alkanes catalyzed by manganese complex $[LMn^{IV}(O)_3Mn^{IV}L](PF_6)_2$ (L = 1,4,7-trimethyl-1,4,7-triazacyclononane) with peroxyacetic acid or H_2O_2 in acetonitrile was first reported as viable by Shul'pin *et al.* in the late 1990s.[73] The reactions catalyzed by $[LMn^{IV}(O)_3Mn^{IV}L](PF_6)_2$ were rationalized by assuming the formation of high-valent metal–oxo intermediates, possibly Mn^{V}=O, in the presence of H_2O_2 oxidant. More interestingly, the stereoselective oxygenation of hexane, cyclohexane, and cycloheptane was dramatically accelerated upon the addition of acetic acid in the $H_2O_2/[LMn^{IV}(O)_3Mn^{IV}L](PF_6)_2$ system. This result suggested the critical role of carboxylic acid additives in improving the product yield and selectivity of asymmetric oxidation reactions.

Likewise, the addition of redox-inactive metal ions, like Al^{3+} as Lewis acids during the generation of Mn^{IV}=O species has shown positive effects on the epoxidation efficiency of non-heme manganese complex, as investigated by Yin *et al.*[74] The effect of adding $Al(OTf)_3$ in the epoxidation of cyclo-olefins and terminal linear olefins catalyzed by $Mn(TPA)Cl_2$ complex (TPA = tris(pyridin-2-ylmethyl)amine) is presented in Table 1 (entry 10–15). For example, the epoxidation of cyclooctene to cyclooctene oxide catalyzed by $Mn(TPA)Cl_2$ catalyst alone has demonstrated sluggish activity, obtaining low product yield and conversion (4.1% and 9.9%, respectively). Under identical conditions, the addition of Al^{3+} generated a much higher oxidation activity with 97.8% conversion and 91.4% yield of epoxide.

Subsequent studies have reported the use of related manganese complexes to catalyze the oxidation of alkene, alcohols, and phenols in both aqueous and organic solutions. Collectively, the factors affecting the generation of active high-valent Mn–oxo intermediates were narrowed down to three points: (1) addition of additives (*i.e.*, carboxylic acid, sulfuric acid, non-redox metal ions as Lewis acids), (2) the number of ligands or *cis*-binding sites available in the structure of the manganese complex, which can bind both of the oxidant and additives, and (3) the nature of reactive intermediates responsible for the catalytic oxidation reaction.[37–39,75] In line with this, Nam *et al.* revealed the role of additives and the nature of active intermediates in Mn complex-catalyzed enantioselective epoxidation of olefins.[76] They employed non-heme Mn catalysts with tetradentate N4 ligand (L^{N4}) (1, Fig. 3a) and pentadentate N5

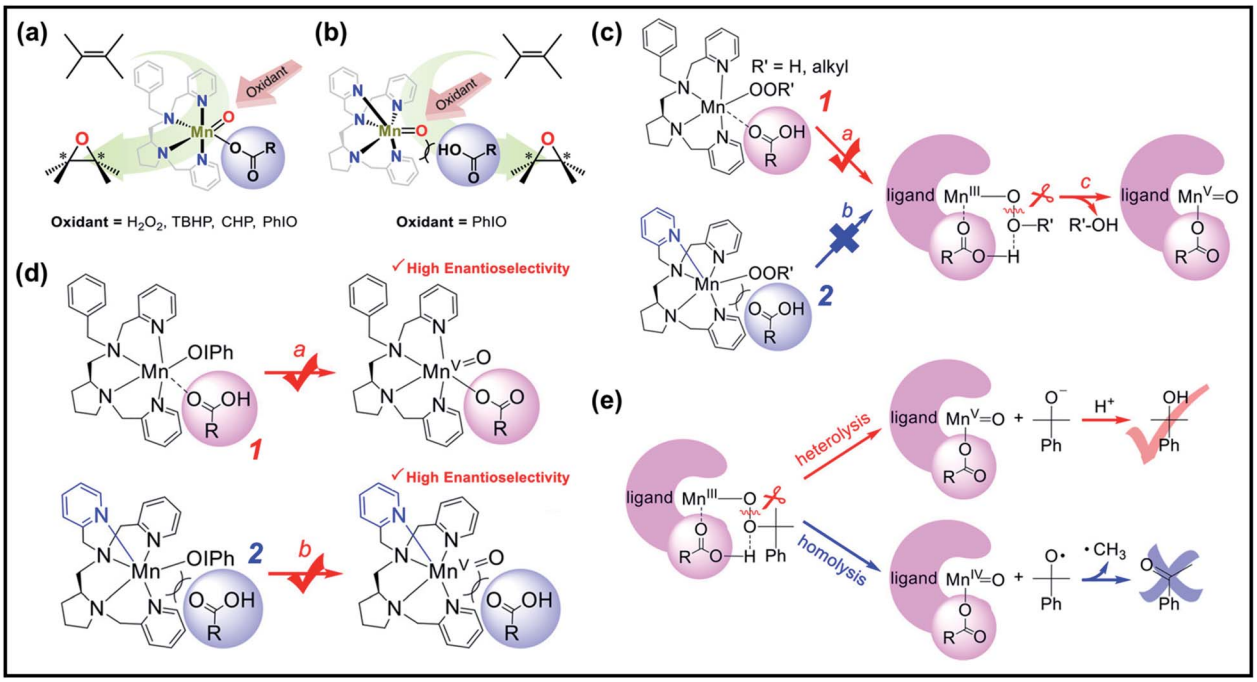

Fig. 3 Asymmetric epoxidation reactions by manganese complexes bearing (a) tetradentate N4 ligands (1) and (b) tetradentate N5 ligands (2). (c) Proposed carboxylic acid-assisted mechanism involving the formation of active manganese–oxo species in the reactions of H_2O_2 and alkyl hydroperoxides. (d) Formation of highly reactive and enantioselective manganese–oxo intermediates during the reactions of **1** and **2** with PhIO in the presence of carboxylic acid. (e) Identification of the mode of O–O bond cleavage of the Mn–(hydro)alkylperoxo intermediate: heterolytic *vs.* homolytic O–O bond cleavage mechanisms. Reproduced with permission.[76] Copyright 2018, American Chemical Society.

ligand (L^{N5}) (2, Fig. 3b), together with H_2O_2, alkyl hydroperoxides, and iodosylbenzene (PhIO) as oxidants, respectively. Fig. 3c and d illustrate the "carboxylic acid-assisted" mechanisms of olefin epoxidation catalyzed by **1** and **2**, respectively. On one hand, it was perceived that when using H_2O_2 and alkyl hydroperoxides as oxidants, only the Mn complex bearing a L^{N4} ligand can bind the carboxylic acid at the manganese center (Fig. 3c, pathway A), which promoted heterolytic O–O bond cleavage (Fig. 3c, pathway C) followed by the formation of highly valent manganese–oxo species. On the other hand, using PhIO as an oxidant, both **1** and **2** catalysts supported the formation of the active manganese–oxo species during asymmetric epoxidation of olefins. Both catalysts obtained high product yields with high enantioselectivity (Fig. 3d). Based on these observations, Nam *et al.* concluded that irrespective of the oxidants in carboxylic acid, the Mn complex with two *cis*-binding sites is the more efficient catalyst. Moreover, the results of their mechanistic studies in olefin epoxidation suggested that a common intermediate (either $Mn^{IV}(O)$ or $Mn^{V}(O)$) was generated as an active species when the reactions using different oxidants were carried out in the presence of carboxylic acid. By conducting a number of stoichiometric and catalytic reactions, it was implicated that $Mn^{V}(O)$ species are more plausible active oxidants in the catalytic oxidation reaction than $Mn^{IV}(O)$ species (Fig. 3e), which is similar to previous proposals.

Furthermore, ruthenium complexes, like ruthenium porphyrin complexes, have also been regarded as efficient catalysts for the epoxidation of olefins. The interest in ruthenium is attributed to its proximity to iron in the periodic table and its ability to generate various high-valent metal–oxo species. Ru^{IV}=O to Ru^{VII}=O species have been postulated to be the most likely active intermediates when olefins are selectively oxidized to the corresponding epoxides *via* oxygen functionalization.[77] Table 1 (entry 16–21) presents some examples of the epoxidation of different alkenes catalyzed by the Ru^{IV}=O intermediate. In this regard, Sheldon *et al.* conducted a comparison study to investigate the reactivity of *cis* and *trans*-Ru^{VI}-dioxo complexes towards the epoxidation of a *trans*-stilbene substrate with sodium periodate ($NaIO_4$) as oxygen donor and ruthenium bis[2-(phenyl azo)pyridine]Cl_2 complex [$(Ru(pap)_2Cl_2)$] as a catalyst.[78] The employed catalyst could be transformed into five isomeric forms, including *trans–trans–trans* (γ), *trans–cis–cis* (α), and *cis–cis–cis* (β) isomers. Both *cis*-β- and *trans*-γ-isomers showed remarkable selectivity for epoxide (47% and 75%, respectively), while the most stable *cis*-α-isomer gave inferior results (34%). The different results observed for the two *cis*-isomers (α and β) were correlated to the steric effect, in which the α-isomer appeared to be more sterically hindered than the β-isomer.

Kojima *et al.* have recently reported a comprehensive review of the characteristics and reactivity of ruthenium oxo complexes towards the oxidation of various organic compounds, including alcohols, alkenes, and alkanes.[54] The authors categorized the synthetic procedures of high-valent ruthenium–oxo complexes into three groups, as shown in Fig. 4a. The formation of the Ru–oxo species can follow either of the following: (1) introduction of a high-valent oxo source into a ligand, (2) employing of an oxo-transfer reagent to oxidize a low-valent Ru complex, and (3) proton-coupled electron transfer (PCET) oxidation of a low-valent Ru–OH_2 complex. As an alternative, Zhang *et al.* recently investigated the potential of dendritic ruthenium porphyrins as a new class of highly selective catalysts for epoxidation and cyclopropanation of alkenes.[79] In their work, poly(benzyl ether) dendritic wedge dendrons (denoted as [G-*n*]) were attached to carbonyl ruthenium^{II}–*meso*-tetraphenylporphyrin (abbreviated as **5**) to form dendritic ruthenium

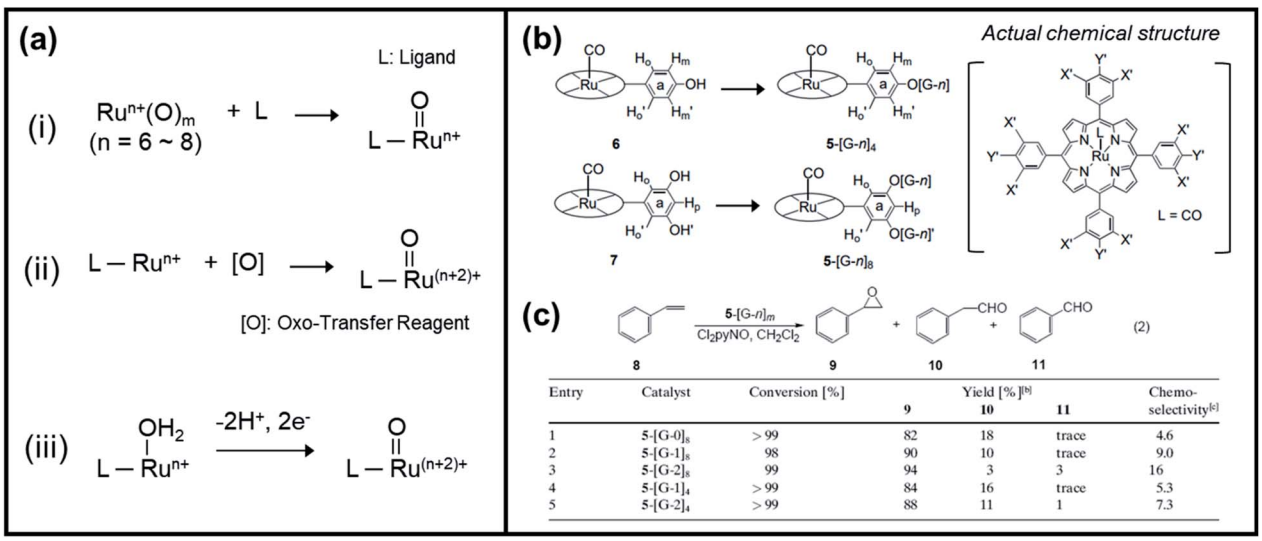

Entry	Catalyst	Conversion [%]	Yield [%][b] 9	10	11	Chemo-selectivity[c]
1	5-[G-0]$_8$	>99	82	18	trace	4.6
2	5-[G-1]$_8$	98	90	10	trace	9.0
3	5-[G-2]$_8$	99	94	3	3	16
4	5-[G-1]$_4$	>99	84	16	trace	5.3
5	5-[G-2]$_4$	>99	88	11	1	7.3

Fig. 4 (a) Categorized synthetic procedures of high-valent ruthenium–oxo complexes. Reproduced with permission.[54] Copyright 2016, The Royal Society of Chemistry. (b) Formation of dendritic ruthenium porphyrins (**5**–[G-*n*]$_4$ ($n = 1, 2$) and **5**–[G-*n*]$_8$ ($n = 0, 1, 2$)) from complex **6** and **7**, respectively, and its actual chemical structure. (c) Catalytic behavior of the dendritic ruthenium porphyrins **5**–[G-*n*]$_m$ toward the epoxidation of styrene (**8**) with excess Cl_2pyNO. Reproduced with permission.[79] Copyright 2002, Wiley-VCH.

porphyrins (**5**–[G-n]$_m$), where n is the generation number of the dendrons (n = 0, 1, 2) and m is the total number of dendrons attached to **5** (m = 4, 8), as displayed in Fig. 4b. It was discovered that the attachment of [G-n] to complex **5** dramatically increased the epoxide yield during the catalytic styrene oxidation reaction. Also, the chemoselectivity of the prepared catalyst significantly increased as the number of attached dendrons increased (Fig. 4c). Notably, prior to this study, there was no inclusive report regarding the dendritic metalloporphyrin catalyzed epoxidation of steroids.

2.3.2. Photochemical routes. Nam *et al.* have shown great interest in the exploitation of water as an oxygen source and solar energy as a driving force for diverse oxygenation reactions.[30] They reported that photocatalytic oxygenation of organic substrates, such as sodium *p*-styrene sulfonate, occurs with nearly 100% quantum efficiency (QE) using Mn^{III}–porphyrin complex, $[Ru^{II}(bpy)_3]^{2+}$ (bpy = 2,2′-bipyridine), $[Co^{III}(NH_3)_5Cl]^{2+}$, and water, as a catalyst, photosensitized electron transfer catalyst, weak one-electron oxidant, and oxygen source, respectively. Briefly, the formation of active Mn–oxo porphyrins $[(Por)Mn^{V}(O)]^{+}$ *via* photoinduced electron transfer assisted by $[Co^{III}(NH_3)_5Cl]^{2+}$ was efficiently mediated by $[Ru^{II}(bpy)_3]^{2+}$ in a phosphate buffer solution (pH 7.4). According to their proposed mechanism, shown in Fig. 5a, the oxidative activation of water is the key step for the development of a photocatalytic electron transfer oxygenation system. Nam *et al.* further investigated the enantioselective epoxidation of terminal olefins *via* a photochemical route using the same reaction system they used in the above study, except for the application of a chiral manganese catalyst, [(*R*,*R*-BQCN)$Mn^{II}(OTf)_2$] (**1**) and synthetic mononuclear non-heme chiral Mn^{IV} oxo complex, $[(R,R\text{-BQCN})Mn^{IV}(O)]^{2+}$ (**2**) where BQCN stands for *N*,*N*′-dimethyl-*N*,*N*′-bis(8-quinolyl) cyclohexanediamine and OTf represent $CF_3SO_3^-$, as displayed in Fig. 5b.[31] Notably, the disappearance of the absorption band at 640 nm (Fig. 5c) upon the addition of vinylcyclohexane to the solution (**2**) and the formation of corresponding epoxide products, with respect to the amount of (**2**), have strongly indicated the involvement of Mn^{IV}–oxo complex as an epoxidizing intermediate in the asymmetric epoxidation of terminal olefins. During the investigation of the mechanistic details for the photochemical route of (**2**) and its reaction with terminal olefins, it was realized that electron transfer (ET) from $[Ru(bpy)_3]^{2+}$* to $[Co^{III}(NH_3)_5Cl]^{2+}$ occurred to give $[Ru^{III}(bpy)_3]^{3+}$ and

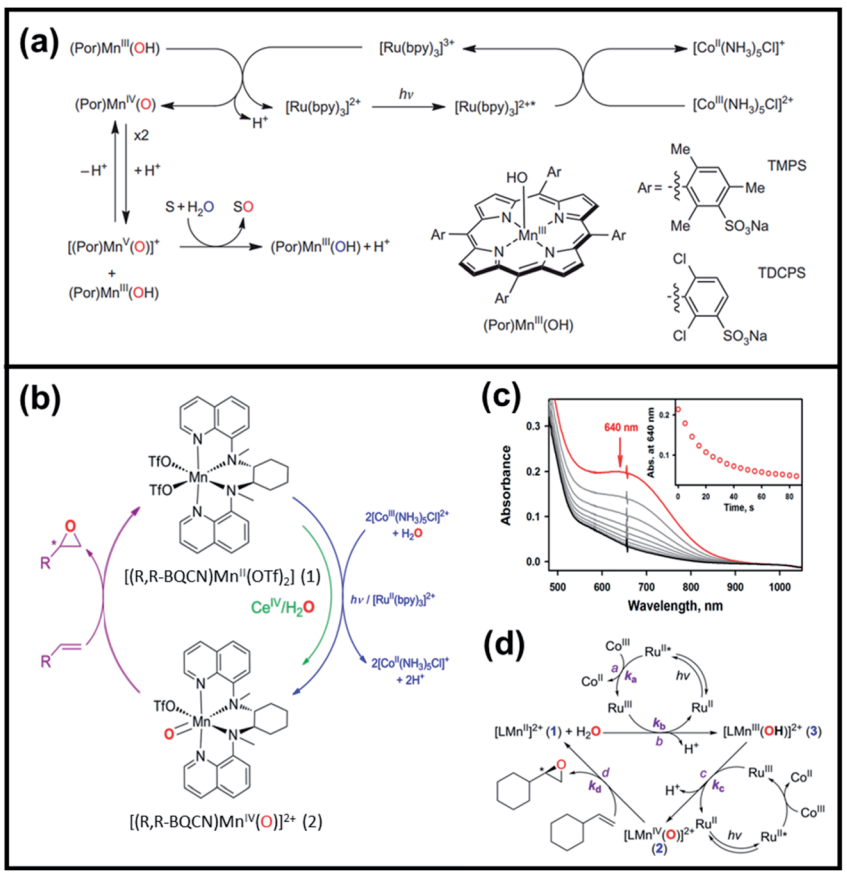

Fig. 5 (a) Proposed reaction mechanism of photocatalytic oxygenation reactions of organic substrates using water, (Por)Mn^{III}(OH), and $[Ru^{II}(bpy)_3]^{2+}$ as the oxygen source, catalyst, and photocatalyst, respectively. Reproduced with permission.[30] Copyright 2011, Macmillan Publishers Limited. (b) Schematic diagram of photocatalytic and stoichiometric enantioselective epoxidation of terminal olefins using Mn^{IV}–oxo complex, (c) UV/vis monitoring of [(*R*,*R*-BQCN)$Mn^{IV}(O)^{2+}$] reacted with vinylcyclohexane (50 mM) in CH_3CN/H_2O solvent (inset shows the decay of the adsorption band at 640 nm), and (d) proposed mechanism of photoinduced generation of non-heme Mn^{IV}–oxo complex and its reaction with olefin. Reproduced with permission.[31] Copyright 2016, American Chemical Society.

Table 2 Catalytic oxidation reactions *via* the photochemical route

Entry	Catalyst	Oxygen source	Substrate	Product	% yield	% conversion [c]
1	(*R*,*R*-BQCN)$Mn^{II}(OTf)_2$ [a]	Water			59 ± 4	53 ± 2
2	(*R*,*R*-BQCN)$Mn^{II}(OTf)_2$ [a]	Water			68 ± 5	50 ± 2
3	(*R*,*R*-BQCN)$Mn^{II}(OTf)_2$ [a]	Water			24 ± 3	57 ± 1
4	(*R*,*R*-BQCN)$Mn^{II}(OTf)_2$ [a]	Water	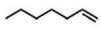	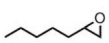	26 ± 3	60 ± 2
5	(*R*,*R*-BQCN)$Mn^{II}(OTf)_2$ [a]	Water	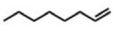	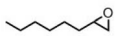	34 ± 4	56 ± 2
6	(*R*,*R*-BQCN)$Mn^{II}(OTf)_2$ [a]	Water			65 ± 5	43 ± 2
7	$[Et_4N][(bTAML)Fe^{III}(OH_2)]$ [b]	Water			90	72
8	$[Et_4N][(bTAML)Fe^{III}(OH_2)]$ [b]	Water	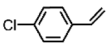	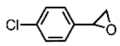	84	50
9	$[Et_4N][(bTAML)Fe^{III}(OH_2)]$ [b]	Water	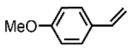	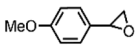	92	95
10	$[Et_4N][(bTAML)Fe^{III}(OH_2)]$ [b]	Water	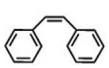	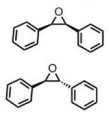	79	58
11	$[Et_4N][(bTAML)Fe^{III}(OH_2)]$ [b]	Water			94	51
12	$[Et_4N][(bTAML)Fe^{III}(OH_2)]$ [b]	Water			92	64

[a] [(*R*,*R*BQCN)$Mn^{II}(OTf)_2$] (BQCN = *N*,*N*′-dimethyl-*N*,*N*′-bis(8-quinolyl)cyclohexanediamine and OTf = $CF_3SO_3^-$).[31] [b] $[Et_4N][(bTAML)\ Fe^{III}(OH_2)]$ (bTAML = biuret-modified tetraamidomacrocyclic ligand).[80]

$[Co^{II}(NH_3)_5Cl]^+$ (Fig. 5d), which influenced the rate of the epoxidation reaction. Table 2 (entries 1–6) summarizes the photocatalytic enantioselective epoxidation of terminal olefins catalyzed by [(*R*,*R*-BQCN)$Mn^{II}(OTf)_2$]. This work might be considered as great progress in the utilization of water as an oxygen source in asymmetric epoxidation reactions.

Subsequently, Gupta *et al.* investigated the selective photocatalytic alkane hydroxylation and olefin epoxidation using high-valent Fe–oxo complex, $[Et_4N][(bTAML)\ Fe^{III}(OH_2)]$ (**1**) as a catalyst, assisted by $[Ru^{II}(bpy)_3]Cl_2$, $[Co^{III}(NH_3)_5Cl]Cl_2$, and water as a photosensitizer, weak one-electron acceptor, and oxygen atom sources, respectively.[80] Fig. 6a displays the proposed catalytic cycle for the photochemical oxygenation reaction catalyzed by the Fe–oxo complex. Upon irradiation with light (3 W blue LED, 440 nm), the iron–oxo complex Fe^{III}–bTAML (**1**) was oxidized to $[(bTAML)\ Fe^{IV}–OH]^-$ which was immediately converted into $[\{(bTAML)Fe^{IV}\}_2(\mu\text{-}O)]^{2-}$ (**2**) dimer. After the addition of a substrate (alkenes or alkanes) to this solution, the dimer (**2**) reacted with the substrate to form $Fe^{V}(O)$ and regenerate the compound (**1**). The formed $[\{(bTAML)\ Fe^{IV}\}_2(\mu\text{-}O)]^{2-}$ (**2**) dimer was revealed as the active oxidant, allowing the hydroxylation of alkanes and epoxidation of alkenes with high selectivity. The photocatalytic hydroxylation of different alkenes by $[Et_4N][(bTAML)Fe^{III}(OH_2)]$ in the presence of water as the oxygen source is summarized in Table 2 (entries 7–12).

The selectivity of the photochemical oxygenation reaction of cyclohexene was considerably improved upon the introduction of homogeneous Ru^{II} porphyrin as a photocatalyst, with water functioning as an oxygen donor.[81–83] Takagi *et al.* recently proposed that the selectivity for epoxidation of alkenes can be further improved using a Ru^{II}–porphyrin–clay hybrid photocatalyst.[84] The authors prepared two types of +2-charged Ru^{II}–carbonyl porphyrin clay-hybrids as sensitizers for the photochemical oxygenation of cyclohexene: (1) $Ru^{II}DMPyP^{2+}$ (5,10-diphenyl-15,20-di(*N*-methylpyridinium-4-yl)porphyrinato ruthenium^{II}-carbonyl dichloride) and (2) $Ru^{II}DMPyMP^{2+}$ (5,10-di[2,6-dimethyl-4-(*N*-methylpyridinium-3-yl)phenyl]-15,20-di(2,4,6trimethylphenyl)porphyrinato ruthenium^{II}-carbonyl dichloride). Note that the carbonyl group coordinated to ruthenium may function as an axial ligand to enhance triplet excited lifetime, which is conducive to photoinduced electron-

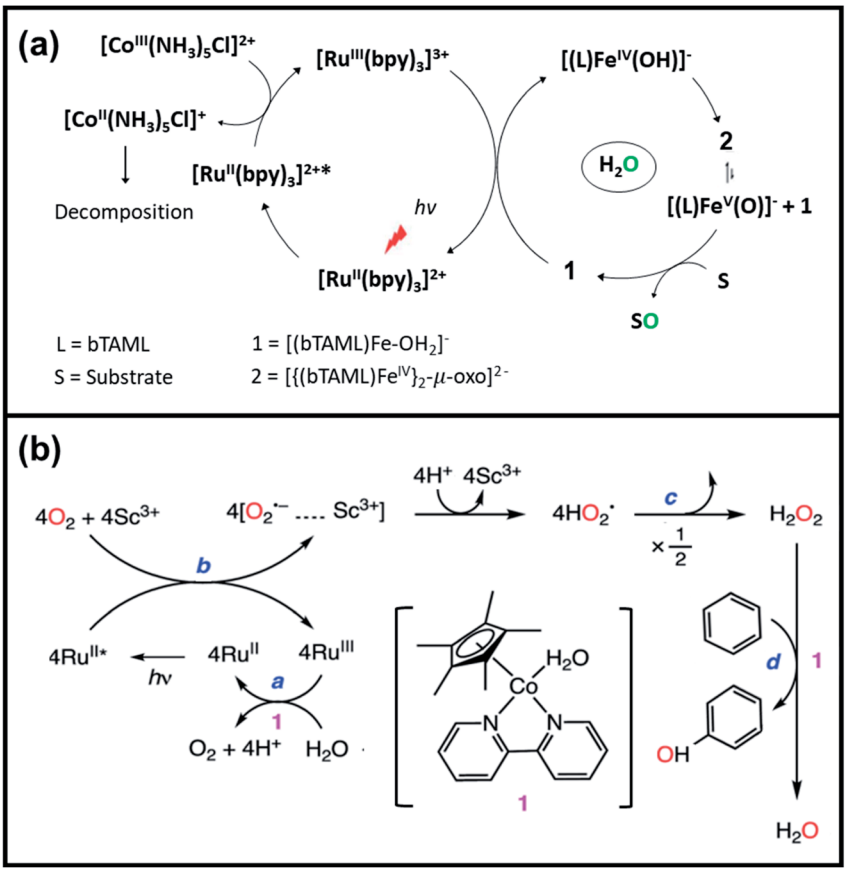

Fig. 6 (a) Proposed reaction mechanism of the selective photocatalytic hydroxylation and olefin epoxidation using $[Et_4N][(bTAML)Fe^{III}(OH)_2]$, $[Ru^{II}(bpy)_3]Cl_2$, $[Co^{III}(NH_3)_5Cl]Cl_2$, and water as catalyst, photosensitizer, one-electron acceptor, and oxygen atom source, respectively. Reproduced with permission.[80] Copyright 2017, The Royal Society of Chemistry. (b) Mechanism of the photocatalytic oxidation of benzene to phenol using dioxygen and water as oxygen and electron source, respectively, in the presence of a cobalt catalyst. Reproduced with permission.[85] Copyright 2017, The Royal Society of Chemistry.

transfer reaction. By performing a photochemical reaction using visible light ($\lambda_{irr.}$ = 420 nm, LED light source), the Ru^{II}DMPyMP^{2+}–clay complex was discovered to work as a longer-lived photocatalyst, attributed to the steric and electronic protection of porphyrin chromophore by 2,6-dimethyl substituents of the phenyl group. The photochemical epoxidation of cyclohexene-sensitive by Ru^{II}–porphyrin-clay hybrid achieved a high selectivity of 96%.

Aside from photocatalytic alkane hydroxylation and olefin epoxidation, photocatalytic oxygenation of benzene and ring-substituted toluene in the presence of O_2 oxidant and water have also shown progress. For example, Fukuzumi *et al.* reported for the first time the photocatalytic hydroxylation of benzene to phenol in the presence of $Sc(NO_3)_3$ under visible light irradiation.[85] They used $[Ru^{II}(Me_2phen)_3]^{2+}$ (Me_2phen = 4,7-dimethyl-1,10-phenanthroline) as photocatalyst and $[Co^{III}(Cp^*)(bpy)(H_2O)]^{2+}$ (Cp = η^5 – penta methyl cyclo penta dienyl) as catalyst for both water oxidation and benzene hydroxylation. Fig. 6b illustrates the mechanism of photocatalytic hydroxylation of benzene to phenol. Specifically, the visible light irradiation of $[Ru^{II}(Me_2phen)_3]^{2+}$ resulted in the formation of H_2O_2 due to photoinduced electron transfer from the excited state of $[Ru^{II}(Me_2phen)_3]^{2+}$ to O_2 oxidant in the presence of Sc^{3+}, as shown in the following equation: $2[Ru^{II}(Me_2phen)_3]^{2+} + O_2 + 2H^+ \rightarrow 2[Ru^{III}(Me_2phen)_3]^{3+} + H_2O_2$. PhOH was then produced *via* the catalytic oxidation of H_2O_2 catalyzed by $[Co^{III}(Cp^*)(bpy)(H_2O)]^{2+}$, in which *p*-benzoquinone product was also detected.

2.3.3. Heterogeneous catalysis. The coinage metals in the periodic table (Cu, Ag, and Au) have shown unique catalytic properties for wide catalytic applications, including CO oxidation, ethylene epoxidation, propene oxidation, and partial oxidation of alcohols.[86] By far, Ag-based catalysts are considered the most efficient for commercialized epoxidation reaction of ethylene with molecular O_2. Generally, the O_2 is adsorbed molecularly on the surface of Ag metal to produce atomic O_2, which is then reacted with ethylene to yield ethylene oxide (EO). However, generated atomic O_2 on the surface of Ag cannot produce more EO as the ethylene substrate or EO itself is being oxidized to CO and H_2O.

Thus, pure Ag metal catalyst can only obtain EO selectivity up to 40–50%.[87,88] The addition of alkali metals like Cs and Re or atomic Cl as additives or inhibitors, to Ag catalyst was found to increase the epoxidation selectivity up to 80%.[89] The selectivity

enhancement is attributed to the partially reversible poisoning of Ag metal surface that hinders the atomic chemisorption of O_2 and therefore impedes the oxidation of ethylene to CO_2 and H_2O.[89] Moreover, optimization of size, shape, and composition of heterogenous Ag-based catalysts have shown promising results.[90–93] For example, Linic *et al.* compared the catalytic performance of Ag nanocubes, pentagonal nanowires, and spherical particles of varying size to demonstrate the impact of chemical and physical factors on the reaction selectivity.[94–96] Fig. 7a–c display high-resolution transmission electron microscopy (HR-TEM) images of an Ag nanowire, nanocube, and the EO selectivity as a function of size and shape of Ag catalysts, respectively. The authors reported that for a given set of external conditions, Ag nanocubes are superior to both nanowires and nanosphere particles and, for a specific particle shape, those with larger sizes have obtained higher EO selectivity. DFT calculations revealed that the difference in the activation barriers is associated with the formation of acetaldehyde and ethylene oxide during epoxidation and is 0.1 eV larger on Ag(100) than on Ag(111). This result suggests that the variation of results among particles of different shapes may be correlated to the exposed crystal facet. Ag(100) facets present in nanocubes intrinsically display higher selectivity towards ethylene oxide compared to Ag(111) facets.

The size effect of Ag catalysts was further investigated by Hensen *et al.* They found that particles larger than 50 nm are composed of multiple Ag crystallites with much smaller domain sizes between 25 and 30 nm.[90] The epoxidation selectivity increased when larger Ag particles exhibited grain boundaries between smaller Ag crystallites, which played a vital role in supplying oxygen atoms to the external surface. Fig. 7d showed the proposed reaction mechanism of Ag-catalyzed ethylene epoxidation. Hensen *et al.* suggested that oxygen atoms from grain boundaries of Ag crystallites slowly dissolve in the bulk Ag and diffuse to the external surface of the catalyst, where they react with ethylene to form ethylene oxide. Thus, the presence of oxygen on the catalyst surface may have stabilized the Ag(111), Ag(110), and Ag(100) facets, and may have induced surface reconstruction.[88,97,98] It was reasoned that the transformation rate of the ethylene is not exactly structure-sensitive, but dependent on the oxygen content of bulk Ag.

Similar to ethylene oxide, propene epoxide (PO) is an versatile chemical intermediates in various chemical industries, including the production of polyether polyols, polyurethane, and propene glycol. Today, the industrial processes for producing PO are the chlorohydrin and the hydroperoxidation (Halcon) processes.[99–103] The major drawback of the former process is the generated chlorinated by-products, which not

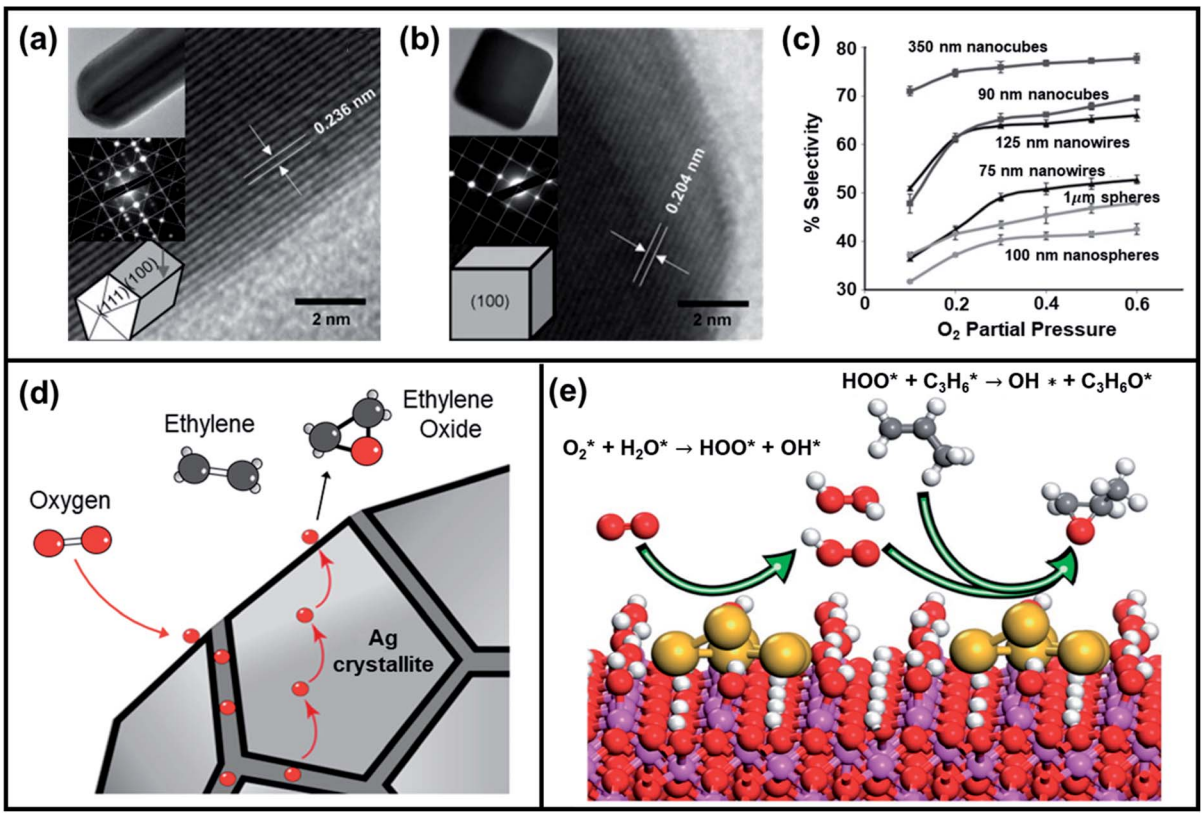

Fig. 7 HRTEM images of a (a) Ag nanowire and (b) Ag nanocube (insets show the zoomed-out TEM images of the nanostructures, selected area electron diffraction patterns, and model structures). (c) Ethylene oxide selectivity as a function of the size and shape of Ag catalytic particles and O_2 partial pressure at 510 K reaction temperature. Reproduced with permission.[95] Copyright 2010, Wiley-VCH. (d) Representative model of Ag catalyst showing the role of grain boundaries for ethylene epoxidation. Reproduced with permission.[90] Copyright 2019, American Chemical Society. (e) Illustration of reaction mechanism of Au-based catalyst (Au/α-Al_2O_3) towards propene epoxidation with O_2–H_2O mixture. Reproduced with permission.[118] Copyright 2016, American Chemical Society.

only impose serious environmental hazards but also destroy equipment due to corrosion.[104–106] Likewise, Halcon process is greatly hindered by the high cost associated with the multiple steps required and low efficiency due to the formation of unwanted by-products, like styrene and *tert*-butyl alcohol. Ideally, propene could be directly oxidized using molecular oxygen assisted by a suitable catalyst. Total and partial oxidation of propene generates propylene oxides with multiple C3 oxygenates, like acrolein, propanal, 1-propanol, isopropanol, and acetone.[107] However, to date, no reported catalyst is being used industrially. Haruta *et al.* were the first to report the potential of nanometer-sized gold clusters dispersed on TiO_2 as an active and highly selective catalyst for direct epoxidation of propene with O_2.[108–110] Since then, the control of Au particle size, support materials, and catalyst preparation methods have been the focus of many studies.[111,112] For example, it was observed that propene molecules adsorbed on adjacent Ti sites generate CO_2 as by-product, and thus, TiO_2 was replaced with titanium silicate (TS-1) as support. Later on, various metal oxides, such as titania, ceria, and iron oxides have also been explored as supports for nanosized Au catalysts.[113–116] In view of synthetic methods for Au catalysts, the best activity was observed for catalysts prepared by the deposition–precipitation method, which gave propene epoxidation selectivity of over 90%.[108,117] Moreover, mechanistic studies showed that the molecular adsorption of O_2 and H_2O on Au clusters could lead to O_2 activation *via* a hydroperoxyl (*OOH) intermediate. To further explicate the mechanism of Au-based catalyst (Au/α-Al_2O_3) towards propene epoxidation with an O_2–H_2O mixture, Li *et al.* applied DFT and *ab initio* molecular dynamics (AIMD) methods.[118] The reaction mechanism is displayed in Fig. 7e. The calculation results demonstrated that *OOH species are readily formed from co-adsorbed intermediates (*O_2 and *H_2O) at the catalyst interface, in which the oxygen molecules prefer the edge of Au clusters while hydrogen actively moves between *OH, *OOH, and *H_2O. The resulting *OOH intermediate was determined to be the key oxidative species, which can be dissociated into atomic oxygen species to produce PO or combined with propene to generate *C_3H_6OOH species that could be easily transformed to epoxypropane.

Silica-supported Au catalysts were then discovered to be capable of catalyzing the selective oxidation of primary and secondary alcohols to aldehydes or ketones using molecular O_2 as the oxidant at atmospheric pressure.[119] In the case of a primary alcohol, 1% Au on the silica support functioned as a surface modifier, which strongly favored the selectivity of aldehydes. However, for the oxidation of secondary alcohols, the Au catalyst acted as a strong activator of organic molecules since the silica support is almost inactive at low temperatures, resulting in a very low conversion rate.

2.4. Overview of non-electrochemical oxygen functionalization

In section 2, we have categorized the non-electrochemical methods for oxygen functionalization into three synthetic routes, namely, chemical routes, photochemical routes, and heterogeneous catalysis. Notably, these non-electrochemical routes have generally exhibited high selectivity and yield. As we discussed in the previous section, the metal–oxo species generated from transition-metal catalysts are considered key intermediate species for most chemical and photochemical studies. In order to generate oxo-species from the initial (resting) state of metal-complex, chemical oxidants or chemical oxidants with photosensitizer are typically added. The appropriate combination of transition metal-based catalysts and chemical oxidants is a vital requirement not only to achieve high selectivity and yield but also to avoid undesirable oxidation reactions such as over-oxidation or oxidation of other functional groups.

In addition, controlling the difference between the redox potential of substrates and metal–oxo species may favor the reaction energetically, hence improve the overall reactivity. Indeed, Nam *et al.* found that the addition of redox-inactive metals to a transition metal complex could modulate the redox potential of metal–oxo species and affected the reactivity.[120] Interestingly, similar phenomena could be found in a biological system, the $CaMn_4$ cluster, an oxygen-evolving complex (OEC) in photosystem II. Agapie *et al.* found that the redox-inactive calcium in the cluster allows a buildup of localized positive charge, modulating the reduction potentials of the Mn in the OEC.[121,122] In this vein, the design of a metal complex with additional hetero atoms or other functional groups could be a prerequisite to expand the scope of oxygen functionalization by a non-electrochemical method.

3. Electrochemical oxygen functionalization

The large energy consumption of modern society produces a significant carbon footprint. This is attributed to the fact that most end products or precursors are formed *via* thermochemical routes. For example, ammonia, a high-volume commodity chemical, is currently produced using the Haber–Bosch process, which proceeds to the reaction of hydrogen (H_2) and nitrogen (N_2) gas under high temperature and high pressure (~500 °C, 150–300 bar). Although it has been regarded as one of the most successful commercialized technologies, it still has major issues, particularly the massive carbon footprint that can reach up to 1.87 tons per ton of ammonia produced.

Electrochemical organic synthesis (also denoted as electroorganic synthesis or organic electrosynthesis) has been studied extensively ever since the first experiments were carried out by Faraday in the 18th century.[123] It has been considered a straightforward and powerful approach for the transformation of organic molecules. Electrochemical organic synthesis is green and environmentally benign, considering external voltage is used as a substitute for toxic redox reagents under mild conditions.[124,125] Unlike the conventional thermochemical route or chemical/photochemical routes, organic electrosynthesis normally does not require any oxidants nor high temperature/pressure. Despite these strong merits, however, only a limited number of commodity chemicals have been produced *via*

electrochemical routes, including anthraquinone, perfluorinated hydrocarbons (PFCs), and adiponitrile.[126,127] Herein, the general aspects of electrochemical organic synthesis are discussed and followed by the developed approaches for this field. The progress of electrochemical oxygen functionalization is shown by the critical assessment of various oxidative electrochemical processes, including the simple ethylene epoxidation reaction and some complex organic substrate functionalization.

3.1. Electrochemical system

3.1.1. Electron transfer mechanism. To appreciate the electrosynthesis phenomena happening between the interface of the electrode surface and reactants, an overview of the electron transfer mechanism should be first discussed. The electroorganic synthesis, including the oxygen-atom functionalization reaction, always follows either two types of electron transfer mechanisms: (1) inner-sphere and (2) outer-sphere electron transfer mechanisms,[124,128–130] as displayed in Scheme 2.

Inner-sphere electron transfer events are always accompanied by the bond formation between the reactant and the electrode surface (catalytic process) within the electrical double layer. This mechanism utilizes a redox-active catalyst, which changes its oxidation state upon the application of an external potential. The oxidized form of this species reacts with the other reactants or substrates to form the desired products. Therefore, the selectivity is largely affected by the chemical reactivity between the reactant and catalyst. Modification of the catalyst surface and properties has been attempted to improve electrochemical performance *via* this mechanism. Conversely, the electron transfer from the electrode to the reactant species is often accompanied by an outer-sphere mechanism, which is simply driven by the applied potential, and no bond formation occurs between the two species (non-catalytic process). The selectivity can only be determined by the potential difference between the electrode and the substrate, in which a redox mediator may help reduce the required overpotential for the process to proceed. It is important to clarify that this type of mechanism may or may not require a redox mediator to facilitate the electron transfer and that the demand for such components solely depends on the electrochemical reaction pathways. The details of this matter are discussed in section 3.2.

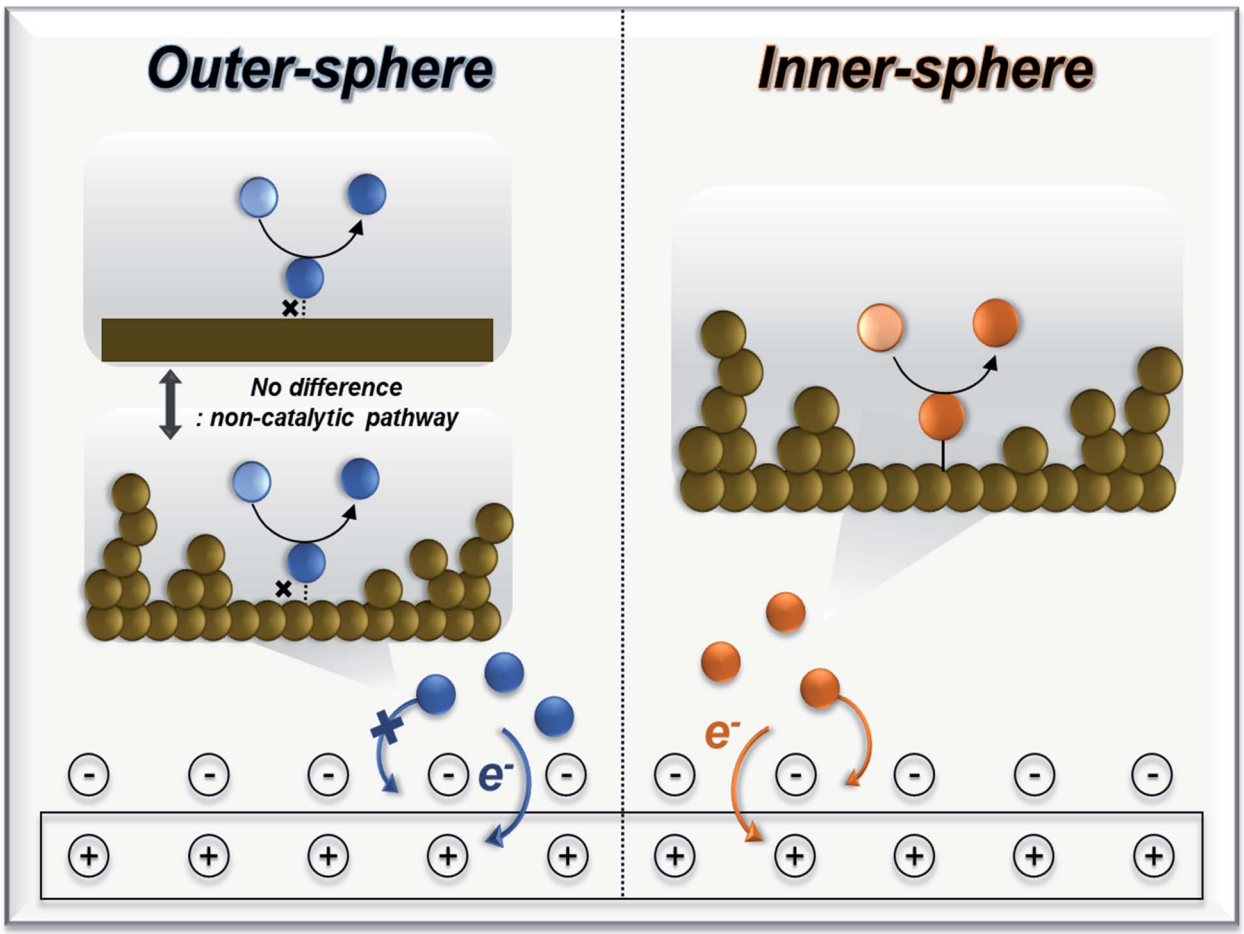

Scheme 2 Schematic diagram of representative electron transfer mechanisms. Briefly, no chemical bonds are formed between reactant/product and electrode surface in the case of outer-sphere electron transfer, thus, electron transfer event occurs outside of electric double layer. On the other hand, inner-sphere electron transfer is accompanied by direct bond formation between reactant/product and electrode surface. Thus, tuning of reactivity can be attained *via* changing the binding affinity of electrode surface toward reactant/product.

3.1.2. Components. The typical configuration of electrochemical organic synthesis is comprised of an electrolyte solution and three electrodes acting as electrical conductors widely known as working electrode (WE), reference electrode (RE), and counter electrode (CE). Two-electrode configuration (only with WE and CE) is sometimes utilized depending on the purpose of the study.[131] Unlike other electrolytic cell reactions, such as water splitting, oxygen reduction, and CO_2 reduction, most organic electrosynthesis requires the use of a non-aqueous medium due to the limited solubility of substrates under aqueous solution. Depending on the application, an electrochemical cell may also contain a membrane separator.[132]

Electrochemical oxygen functionalization reactions require the following components: organic substrates, oxygen atom sources, redox mediators (or electrocatalysts), and reaction media (solvents and supporting electrolytes). Redox mediators (also referred to as redox catalysts, electron transfer mediators, or just mediators) are species soluble in electrolytes that have redox activity in a typical working potential window. Redox mediators act as charge carriers, they are reduced/oxidized at the electrode surface and are then transferred from the reaction site and chemically react with O_2.[133] From a mechanistic point of view, redox mediators play three key roles in electrochemical reaction systems: (1) facilitating the transfer of electrons between the anode and organic substrate to improve electrokinetics, (2) lowering the overpotential needed for radical generation, and (3) controlling the selectivity of the chemical steps that occur after electron transfer.[134] An activated form of the mediator is generated (Med_{ox}) when the applied potential reaches the redox potential of the mediator (E_{med}). A charge transfer process occurs between Med_{ox} and the substrate to generate highly reactive radicals or cations as intermediate species, followed by the formation of desired products. Based on this, several criteria of the appropriate mediator were recently suggested.[124,135] For example, the redox potential of the mediator must be lower than that of the substrate so as to not allow the substrate to be oxidized or reduced. However, the potential difference between the two components should not be large lest the reaction rates become impractically slow. More importantly, both the reduced and oxidized form of the mediator should be inert to all processes other than electron transfer since irreversible side reactions dramatically reduce the catalytic activity. Lastly, the solubility of these transformed species must be high enough to ensure homogeneity throughout the electrolysis period.

Reaction media such as solvents and supporting electrolytes play significant roles in the control of electrochemical reactions. These components serve as an environment for molecular events, such as electron transfer and subsequent chemical processes, including the separation and extraction of products from reaction mixtures. Acetonitrile (ACN), dimethylformamide (DMF), and tetrahydrofuran (THF) are generally used with a supporting electrolyte.[136–139] However, these compounds are destructive to both human health and the environment. In this vein, ionic liquids and supercritical fluids are being regarded as alternative reaction media for organic electrochemical reactions.[140–146] Their primary advantages include low vapor pressure, nonflammability, high polarity, and relative inertness, whereas these reaction media are costly although they can be recovered and reused after reactions.

3.2. Proposed electrochemical pathways

The progress of electrochemical oxygen-atom functionalization has led to the development of three routes, as follows: (1) direct electro-oxidation *via* outer-sphere electron transfer, in which reagent-electron transfer is conducted on the electrode surface; (2) indirect electro-oxidation in presence of redox mediator to facilitate the activation of the substrate; and (3) direct electro-

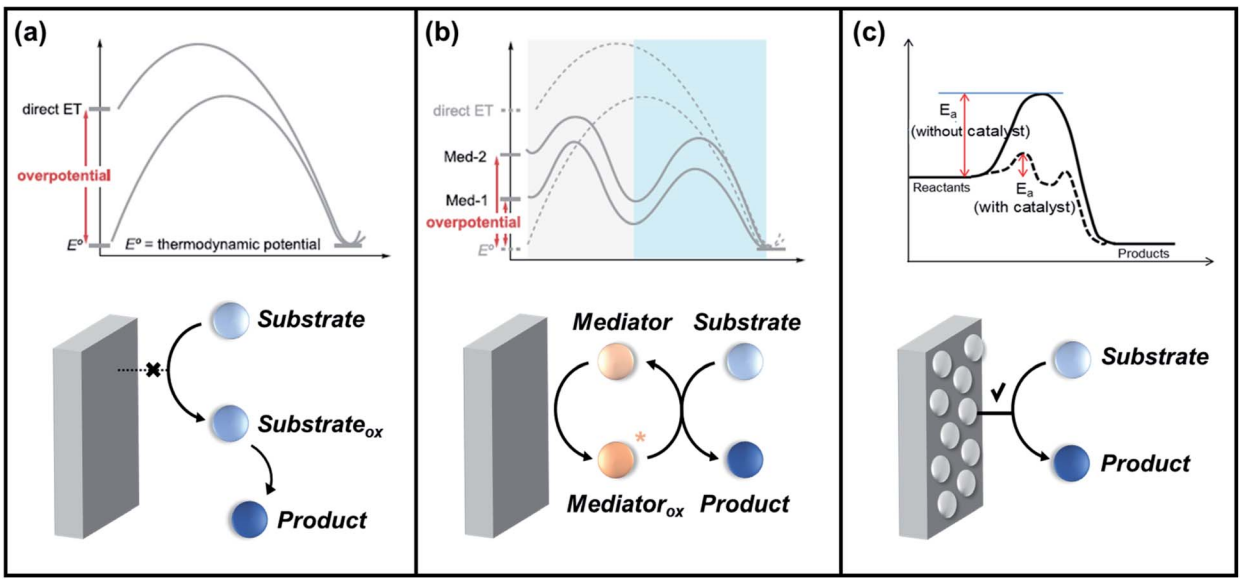

Scheme 3 Simplified energy profiles and schematic diagrams for (a) direct electro-oxidation *via* the outer sphere mechanism, (b) indirect electro-oxidation with mediators, and (c) direct electro-oxidation *via* the inner sphere mechanism. Reproduced with permission.[125,147] Copyright 2020, American Chemical society and Copyright, 2020 MDPI.

oxidation *via* inner-sphere electron transfer, which employs an electrocatalyst to mediate the transformation of the organic substrate. Scheme 3 shows schematic diagrams and simplified energy profiles of the three electro-organic synthesis pathways to demonstrate their differences.[125,147]

3.2.1. Direct electro-oxidation *via* outer-sphere electron transfer. The direct electro-oxidation pathway following an outer-sphere mechanism is a non-catalytic process as the applied potential is directly used to activate the substrate. Briefly, the substrate molecules immediately interact with the electrode surface *via* outer-sphere electron transfer, which induces the formation of unstable radical cations and anions as intermediates (Scheme 3a). These intermediates accumulate on the space near the electrode surface, commonly known as the formation of double (or polymer) layer which pertains to electrode fouling.[148] This phenomenon is specifically observed during direct electro-oxidation at low anodic potentials, in which the reaction rate is usually slow. Consequently, to avoid the electrode fouling during direct electro-oxidation of organic compounds, relatively high anodic potentials are applied. This process does not require any catalysts or mediators to activate the substrate, but the high kinetic barrier greatly hinders the potential application of this pathway.[123,149]

In search for efficient electrochemical approaches where the substrate and electrode could interact directly to generate reactive and valuable species, Patureau *et al.* designed a metal- and chemical oxidants-free electro-oxidation process to produce aromatic esters.[150] Initially, the group investigated 4-methylanisole as the model substrate reacting with methanol in an undivided cell, composed of carbon as anode and nickel as cathode. Upon the application of potential, three compounds were formed including the target oxidative coupling product ester, aldehyde, and acetal. Fig. 8a shows the proposed mechanism of the production of ester products. By passing an electric current to the substrate (**a**), an aryl radical cation (**a′**) is formed at the anode followed by deprotonation and oxidation, which eventually forms a quinone methide derivative (**a″**). Further anodic oxidation events lead to the formation of acetal intermediate (**e**). The direct electro-oxidation of this intermediate species at the anode side would then generate the ester product (**c**). Importantly, the proposed electro-oxidative method to construct esters and acetals from methylarenes and benzaldehydes offers a new approach in synthetic chemistry. Likewise, Chiba *et al.* reported a selective functionalization of styrenes with O_2 into carbonyls products.[151] The group suggested the plausible mechanisms of olefin cleavage *via* direct anodic oxidation of styrene, as shown in Fig. 8b. The production of carbonyl products *via* the olefin cleavage of styrene substrate (**2a**) may follow two pathways. Initially, a styrene radical cation intermediate ($\mathbf{2a}^{\bullet+}$) with trapped $O_2^{\bullet-}$ species would be formed upon the application of potential. Subsequently, dioxetane intermediate (major pathway) and epoxide intermediate (minor pathway) are formed, whereas the former species is immediately decomposed into the target carbonyl compounds.

3.2.2. Indirect electro-oxidation with mediators. To overcome the difficulties of the direct electro-oxidation route, indirect electro-oxidation (also known as a mediated route) has been broadly studied. This alternative pathway utilizes redox mediators to accelerate electron transfer between substrate molecules and the electrode surface, as shown in Scheme 3b. This pathway can alter the shape of the energy diagram and reduce the required overpotential, thereby allowing the reaction to proceed at milder conditions with higher selectivity.[152,153] In particular, the electrochemical oxidation of halides is a facile way to prepare oxidant species (Br_2, I_2, and Cl_2) that can be used as electron transfer mediators. It involves the reaction of halogens or halides with a substrate leading to the formation of intermediate compounds that are readily converted to target products.[154] Note that halides are recognized as strong mediators for electrochemical oxidation, which is attributed to their ability to hold one more electron in a p-orbital. Torii *et al.* have put much effort into investigating the halogen-mediated electrochemical route,[155–157] including the report about the selective conversion of olefins into epoxides, bromohydrins, and dibromides using sodium bromide (NaBr) in water-organic solvent electrolysis systems, (MeCN–H_2O–NaBr-(Pt)).[155] The electro-

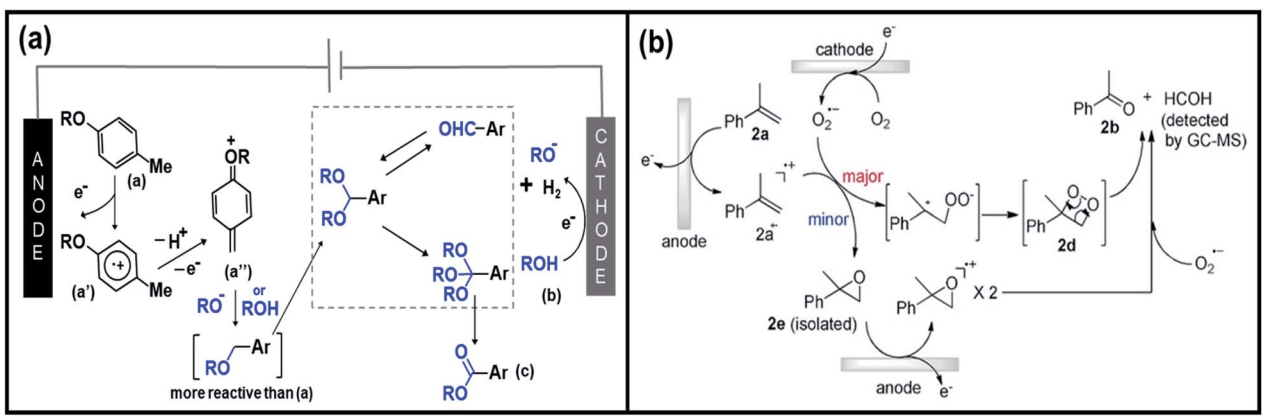

Fig. 8 (a) Illustration of the proposed mechanism of direct electro-oxidation of methylarenes to ester products. Reproduced with permission.[150] Copyright 2020, Wiley-VCH. (b) Plausible mechanisms of olefin cleavage *via* direct anodic oxidation of styrene. Reproduced with permission.[151] Copyright 2019, Wiley-VCH.

halo-functionalization of olefins in this system proceeds *via* different pathways, in which the acidity of the electrolysis media and the concentration of bromide salts have directly influenced product formation and yield. They also established the chemical and electrocatalytic asymmetric dihydroxylation of various olefins using iodine (I_2) as a capable oxidizing mediator in I_2–K_2CO_3–$K_2Os_2(OH)_4$ and I_2–K_3PO_4/K_2HPO_4–$K_2Os_2(OH)_4$ electrolysis systems, respectively.[156] Under different conditions in an integrated electrochemical cell, I_2 acted as a recyclable co-oxidant for potassium osmate, leading to higher yield and % enantiomeric excess (% ee). This insight encouraged the development of enantioselective electro-epoxidation of olefins by using an optically active Cl^-/Mn-complex as a mediator in a CH_2Cl_2 aqueous NaCl two-phase system.[157] The anodic oxidation of Cl^- leads to ClO^- active species, which transfer the CH_2Cl_2 phase and work as an adequate co-oxidant to generate and regenerate multiple times the optically active Mn=O complex, as shown in Fig. 9a. The overall electrochemical process has achieved yields and % ee of epoxides that were almost comparable to those obtained from chemical epoxidation, as shown in Table 3. Subsequently, the production of epoxides has followed the halogen-mediated route for a long time due to high efficiency. However, the overall process is not economically viable because of the formation of by-products.

Alternatively, hydrogen peroxide (H_2O_2) has been considered one of the environmentally benign oxidants for electro-organic synthesis since the by-product being produced is only water.[158,159] However, H_2O_2 is usually produced through the anthraquinone process, which requires toxic solvents to regenerate the employed catalysts, contradictory to the originally intended function of H_2O_2. Also, the hazards associated with the storage and transportation of concentrated H_2O_2 have been a hindrance to the progress of this approach. One solution proposed is to produce low strength H_2O_2 by electrochemical reduction of O_2, which offers an alternative way to utilize this oxidant. A particular example is the investigation of Ho *et al.* regarding the electro generation of H_2O_2 in [bdmim][BF_4] IL (ionic liquid), followed by the *in situ* epoxidation of electrophilic alkenes in the $H_2O_2/HCO_3^-/Mn^{II}$ system, represented in Fig. 9b.[160] Notably, the addition of water in the [bdmim][BF_4]/NaOH mixture resulted in the efficient production of H_2O_2, while the introduction of CO_2 in the H_2O_2/[bdmim][BF_4]/NaOH(aq) with Mn^{II} catalyst generated the peroxymonocarbonate anion, HCO_4^-, which was suggested to be the active species corresponding to the epoxidation. The ionic liquid was recovered and reused multiple times without showing significant changes in electrochemical performance, which is significant since the IL is the most expensive component in the proposed system. Table 4 summarizes the epoxidation of various lipophilic alkenes in H_2O_2/[bdmim][BF_4]/NaOH(aq) reaction media and Mn^{II} catalyst.

3.2.3. Direct electro-oxidation *via* inner-sphere electron transfer. Note that most oxidation reactions in electro-organic synthesis are likely to proceed *via* two-electron processes, in which single-electron transfer (SET) from organic molecules generates high-energy radical cations as intermediates. These

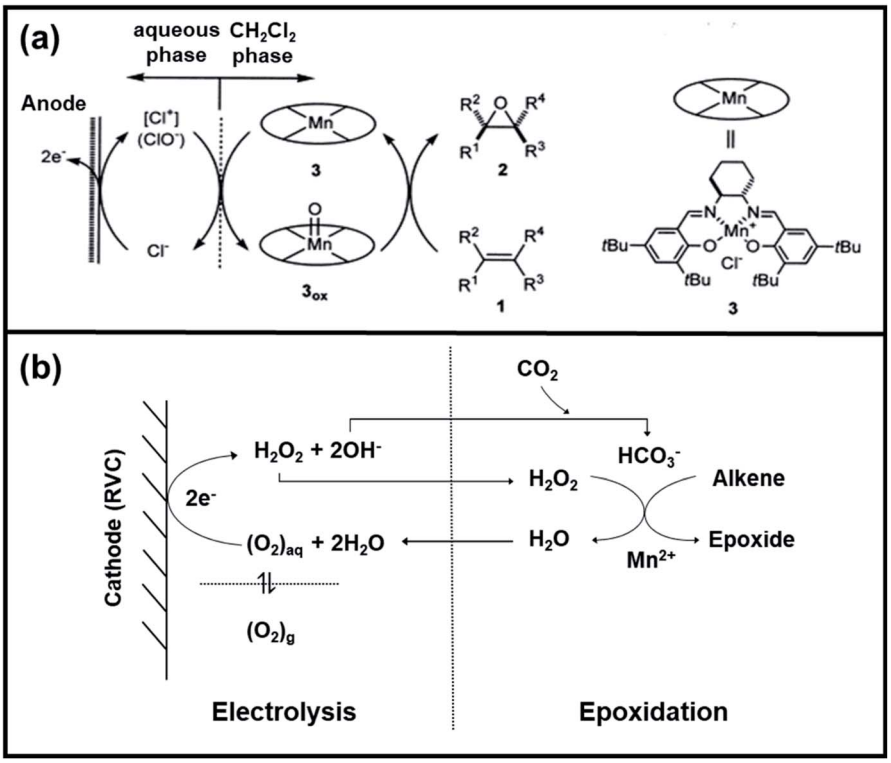

Fig. 9 (a) Possible reaction mechanism of Mn–salen complex mediated electro-epoxidation of olefins water/CH_2Cl_2 two-phase system. Reproduced with permission.[157] Copyright 2001, Elsevier Science B.V. (b) Coupling of the electrogeneration of H_2O_2 in [bdmim][BF_4] ionic liquid with the manganese/bicarbonate-activated epoxidation system. Reproduced with permission.[160] Copyright 2006, Elsevier Ltd.

Table 3 Catalytic oxidation reactions *via* the electrochemical route using an optically active Cl^-/Mn-complex as a mediator in a CH_2Cl_2 aqueous NaCl two-phase system

Entry	Catalyst	Oxidant/electrolyte	Substrate	Product	% yield	% conversion[b]
1	Mn-salen$_3$[a]	CH_2Cl_2/NaCl			93	87[b]
2	Mn-salen$_3$[a]	CH_2Cl_2/NaCl	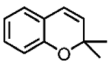	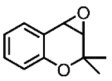	80	81[b]
3	Mn-salen$_3$[a]	CH_2Cl_2/NaCl			69	43[b]
4	Mn-salen$_3$[a]	CH_2Cl_2/NaCl	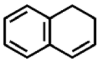	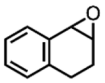	47	40[b]
5	Mn-salen$_3$[a]	CH_2Cl_2/NaCl		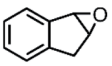	30	26[b]

[a] (*S*,*S*)-*N*,*N*-bis(3,5-di-*tert*-butylsalicylidene)-1,2-cyclohexanediaminomanganese^{III} chloride.[157] [b] % enantioselective epoxide.

intermediates demand high electrode potentials, which severely restrain the utility of many of the electrochemical organic oxidation reactions. To alleviate this hindrance, various forms of electrocatalysts have been applied during the direct electrooxidation route to lower the kinetic barrier existing in oxidation and reduction reactions, which subsequently follows an

Table 4 Catalytic oxidation reactions of various lipophilic alkenes *via* the electrochemical route using Mn^{II} catalyst in H_2O_2/[bdmim][BF_4]/NaOH(aq) reaction media

Entry	Catalyst	Oxidant/electrolyte	Substrate	Product	% yield	% conversion
1	Mn_sO_4/HCO_3	H_2O_2/IL/NaOH[a]			83	>99
2	Mn_sO_4/HCO_3	H_2O_2/IL/NaOH[a]		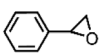	84	>99
3	Mn_sO_4/HCO_3	H_2O_2/IL/NaOH[a]			80	>99
4	Mn_sO_4/HCO_3	H_2O_2/IL/NaOH[a]	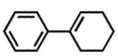	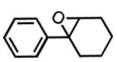	90	>99
5	Mn_sO_4/HCO_3	H_2O_2/IL/NaOH[a]			83	95
6	Mn_sO_4/HCO_3	H_2O_2/IL/NaOH[a]			76	87
7	Mn_sO_4/HCO_3	H_2O_2/IL/NaOH[a]	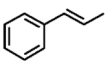	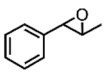	71	81
8	Mn_sO_4/HCO_3	H_2O_2/IL/NaOH[a]		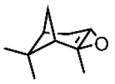	62	75
9	Mn_sO_4/HCO_3	H_2O_2/IL/NaOH[a]	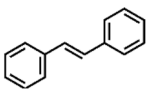	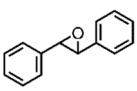	42	44

[a] Ionic liquid, [bdmim][BF_4].[160]

inner sphere electron mechanism (Scheme 3c). The selectivity *via* this advanced route is determined by the chemical reactivity between the substrate and the electrocatalyst. As mentioned earlier, electrocatalysts are beneficial for reducing the overpotential needed for radical generation and for expediting the transfer of electrons between the anode and organic substrate. Although numerous electrocatalysts were already developed and synthesized by many respected groups in the past, the overall performance of electro-organic synthesis *via* this route is still very much restricted. Recently, Manthiram *et al.* utilized the water molecules to electrochemically synthesize the epoxides from olefin substrates.[161] They proposed ideal direct electro-oxidation using water as the oxygen-atom source and monodisperse manganese oxide (Mn_3O_4) nanoparticles for the synthesis of greener and safer target products.[162] The feasibility of the suggested direct electrochemical oxidation is clearly shown in Fig. 10a. This figure shows the thermodynamics analyses of their proposed reaction, wherein the conversion of ethylene-to-ethylene oxides did not occur, even at high temperature and pressure (thermochemical route), while the obvious formation of epoxides was easily depicted upon the application of voltage. In addition, Fig. 10b demonstrates the proposed mechanism for direct electrochemical epoxidation of cyclooctene using Mn_3O_4 NPs as electrocatalysts and water as the sole oxygen atom source. Manthiram *et al.* hypothesized that upon addition of cyclooctene to the Mn^{IV}=O species (resting state of Mn_3O_4 NPs), cyclooctene oxides are formed together with Mn^{II}-vacant sites. Accordingly, the nucleophilic attack of water to the available Mn^{II} sites is suggested as the rate-determining step of the reaction, which induced the

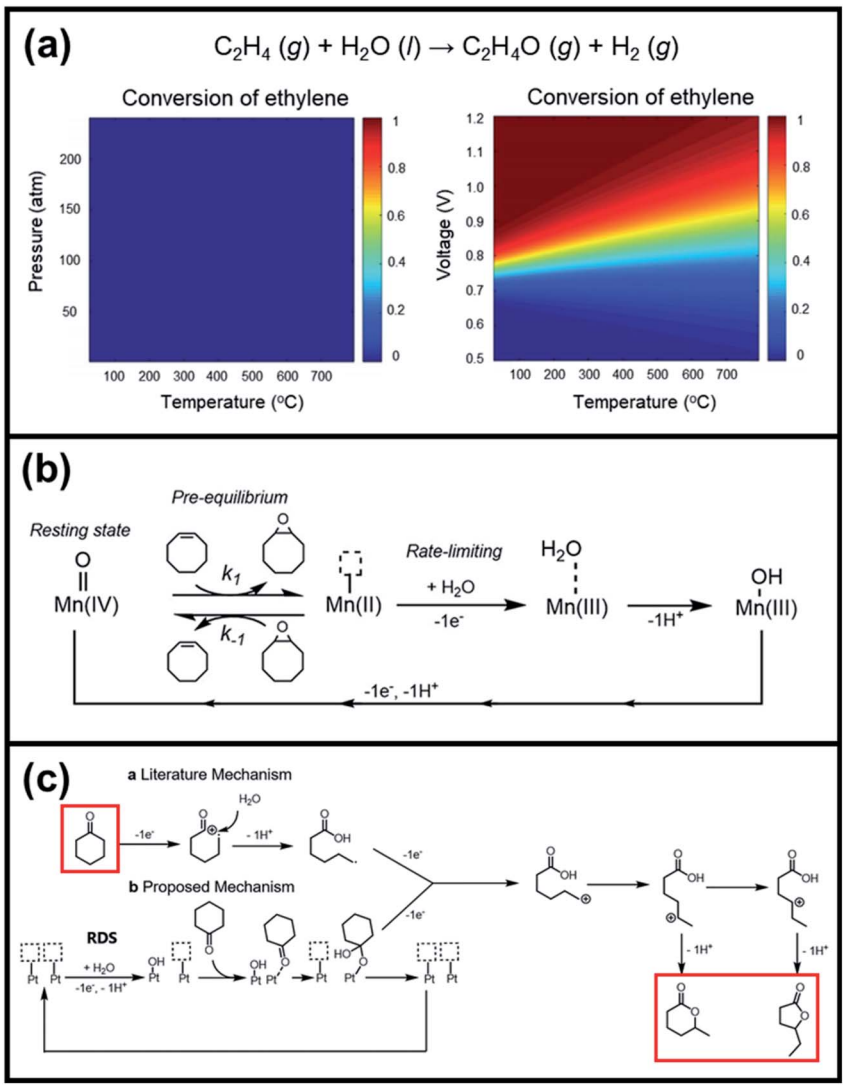

Fig. 10 (a) Analyses of the conversion of ethylene to ethylene-oxides through the thermochemical route and electrochemical route. (b) Suggested mechanism for electrochemical epoxidation of cyclooctene using Mn_3O_4 nanoparticles as oxidation catalysts and water as an oxygen atom source. Reproduced with permission.[162] Copyright 2019, American Chemical Society. (c) Proposed mechanism for electrochemical lactonization of cyclic ketones using Pt foil electrodes and water as an oxygen atom source. The rate-determining step involves the activation of water molecules by Pt in an electron transfer to form Pt–OH. Reproduced with permission.[163] Copyright 2020, American Chemical Society.

Table 5 Catalytic oxidation reactions *via* the electrochemical route using Mn_3O_4 nanoparticles and dirhodium^{II} caprolactamate, respectively

Entry	Catalyst	Oxidant/electrolyte	Substrate	Product	% yield	% conversion
1	Mn_3O_4 NPs	Water			28.3[a]	55.1[a]
2	Mn_3O_4 NPs	Water			18.9[b]	30.2[b]
3	$Rh_2(cap)_4$[c]	CH_2Cl_2/^{t}BuOOH	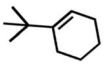	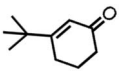	94	N.D.
4	$Rh_2(cap)_4$[c]	CH_2Cl_2/^{t}BuOOH	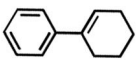	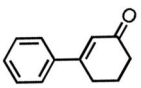	77	N.D.
5	$Rh_2(cap)_4$[c]	CH_2Cl_2/^{t}BuOOH	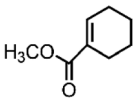	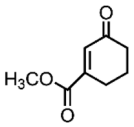	92	N.D.
6	$Rh_2(cap)_4$[c]	CH_2Cl_2/^{t}BuOOH		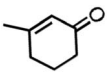	75	N.D.
7	$Rh_2(cap)_4$[c]	CH_2Cl_2/^{t}BuOOH	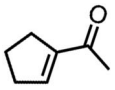	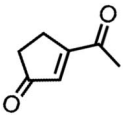	86	N.D.
8	$Rh_2(cap)_4$[c]	CH_2Cl_2/^{t}BuOOH	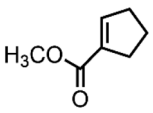	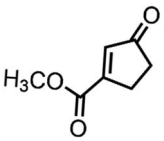	79	N.D.

[a] $n = 8$. [b] $n = 7$.[162] [c] $Rh_2(OAC)_4$ with anhydrous TBHP (*tert*-butyl hydroperoxide).[174]

formation of Mn^{III}–OH_2 accompanied by a one-electron transfer. The suggested alternative electro-oxidation route not only anticipated the utilization of water for the electrochemical epoxidation reaction at ambient conditions, but also projected a lower kinetic barrier associated with the use of suitable electrocatalysts. However, low conversion efficiencies (30% of the maximum theoretical efficiency), shown in Table 5 (entries 1 and 2), were initially achieved and more efforts are still necessary to fully unfold the potential of this innovative direct electrooxidation.

Manthiram *et al.* then investigated the possibility of electrochemical lactone formation by following the same concept of their previous study.[163] In their proposed reaction mechanism (Fig. 10c), the water molecule is initially activated on a Pt electrode surface following an inner-sphere electron transfer to form Pt–OH. The adsorbed OH species then reacts with the adsorbed cyclohexanone to form an active intermediate, which can proceed to the formation of carboxylic acid cation *via* ring-opening electron transfer. By extending the electrochemical oxidation, the formed cation can carry on to ring-closure, thus forming lactone products. Isotope labeling experiments verified that the oxygen in the lactone products is inserted into cyclohexanone from the water in the electrolyte, with hydrogen gas co-produced at the cathode. With the use of water as the sole oxygen atom source, the authors were able to produce lactones from cyclohexanone with faradaic efficiencies of approximately 20%.

However, aside from the low conversion efficiencies obtained from initial experiments, the identification of conditions under which the desired reaction proceeds selectively imposes a major technical challenge for this electrochemical approach. Specifically, the lack of profound comprehension regarding the involved reaction, including the electron and proton movement, rate of oxygen functionalization from the reactant to the surface of the catalyst, and the role of the catalysts, is a major concern of direct electrooxidation following an inner-sphere mechanism. It is then imperative to address these issues to optimize the overall performance of direct electrochemical oxidation in terms of conversion, faradaic efficiency, yield, and selectivity.

3.3. Oxygen functionalization by electrochemical methods

3.3.1. Epoxidation. Electrochemical oxidation and functionalization of simple olefins such as ethylene, propylene, and butene by means of C=C bond cleavage and addition of oxygen

atoms can give rise to valuable products, including epoxides, ketones, 1,2-diols, aldehydes, and carboxylic acids. Notably, the anodic oxidation of these low-cost unsaturated hydrocarbons can proceed with or without a redox mediator. Metal–oxo catalyst systems employing iron, ruthenium, manganese, chromium, and osmium metals are commonly used mediators in the electrochemical oxygenation of olefins. The chemistry of metal–oxo complexes has been extensively studied for non-electrochemical methods, as these species are capable of initializing several types of transformations, such as oxygen functionalization and hydrogen abstraction of strong C–H, N–H, and O–H bonds. This section of the review presents the promising transformation of olefin substrates *via* electrochemical oxygen functionalization.

The direct chemical reaction between oxygen and olefins is the conventional method to synthesize various epoxides, however, this process is economically challenged by the harsh reaction conditions and formation of unwanted by-products. Driven by these limitations, Van der Eijk *et al.* established the first non-conventional route involving the electrochemical oxidation of higher olefins into their respective epoxides.[164] The challenge of this approach is the identification of conditions under which the desired reaction proceeds selectively. As a response, an electrochemically generated Ag^{II}–pyridine ($Ag(Py)_2^+$) was employed as a mediator to selectively oxidized propene and four isomeric butenes. Taking propene saturated in a silver acetate solution as an example, they demonstrated that upon electrolysis, Ag^I was oxidized to a Ag^{II} complex, then this complex was readily reacted with propene to give Ag^I and propene oxide. Eqn (1)–(3) summarize the involved reaction mechanism.

$$Ag(Py)_2^+ + 2Py \rightarrow Ag(Py)_4^{2+} + e^- \quad (1)$$

$$2Ag(Py)_4^{2+} + H_2O \leftrightarrow Ag(Py)_2^+ + Ag(Py)_2O^+ + 4Py + 2H^+ \quad (2)$$

$$Ag(Py)_2O^+ + C_nH_{2n} \rightarrow Ag(Py)_2^+ + C_nH_{2n}O \quad (3)$$

Van der Eijk *et al.* confirmed that the rate-determining step in the electrochemical epoxidation of higher olefins is the transfer of an electrophilic oxygen atom from the mediator to the homogeneously dissolved substrates. Importantly, their results brought out the potential of Ag^{III} oxides as a competent selective epoxidation agent for higher olefin substrates.[165,166]

Moreover, ruthenium complexes, such as ruthenium porphyrin complexes, have been regarded as efficient electrocatalysts for the epoxidation of olefins due to the accessibility of high-valent ruthenium–oxo species (Ru^{IV}=O to Ru^{VII}=O). These species were presumed to be the most likely active intermediates when olefins are selectively oxidized to the corresponding epoxides *via* oxygen functionalization.[77,78] Krtil *et al.* recently reported regarding the electrocatalytic ethene epoxidation on nanocrystalline RuO_2 interesting to discuss in detail.[167] The electrocatalytic properties of the Ru-based oxides

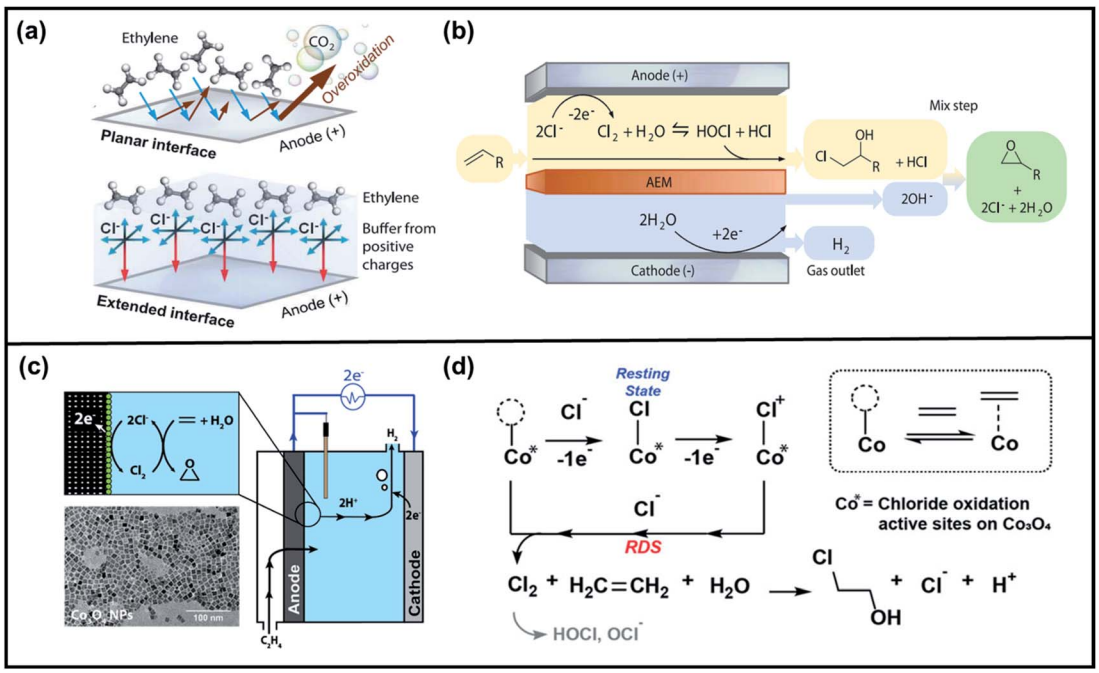

Fig. 11 (a) Schematic diagram illustrating ethylene oxidation at a planar interface (leading to overoxidation) and the proposed chloride-mediated selective electrosynthesis that presents an extended interface and (b) the chloride-mediated electrochemical system of ethylene to ethylene-oxide transformation, in which the formation of ethylene chlorohydrin in the anolyte and the generation of ethylene oxide in the mixing step are proposed. Reproduced with permission.[168] Copyright 2020, American Association for the Advancement of Science. (c) Schematic of an electrochemical ethylene oxidation cell (inset shows the mechanism of electrochemical epoxidation and TEM image of Co_3O_4 nanoparticles) and (d) the proposed mechanism for chlorine-mediated electrochemical ethylene oxidation in saline water. Reproduced with permission.[169] Copyright 2020, American Chemical Society.

were tuned by controlling the particle size and by doping with Co. However, they realized that CO_2 is the main ethene oxidation reaction product on nanocrystalline RuO_2 and $Ru_{0.8}Co_{0.2}O_2$ electrodes in acid media. To shift the reaction pathway, they employed the Cl^- ion as a surface blocking agent, which effectively cut-off the CO_2-reaction channel due to the formation of Ru–O–Cl surface species. Such hindrance to the formation of CO_2 allowed the production of ethylene oxide in acid media. The sudden appearance of this product above the potential of approximately 1.2 V upon the addition of 0.3 M Cl, was explained through DFT calculations, which showed that the lone surface oxygen sites (Ru–O) surrounded by Cl^- ions are the active species responsible for the epoxidation process. Accordingly, Cl was confirmed as an efficient epoxidation promoter that switches off the combustion pathway toward CO_2 and enables the epoxidation reaction channel by surface reactive site blocking.

Sargent *et al.* recently reported chloride-mediated selective electrosynthesis of ethylene and propylene oxides at high current density under ambient conditions.[168] They postulated that chloride is likely an efficient redox mediator at the anode that facilitates the selective partial oxidation of ethylene to ethylene oxide. As shown in Fig. 11a, the extended heterogeneous/homogeneous interface induced by the Cl^- ions can buffer ethylene from uncontrolled oxidation, leading to the production of ethylene oxide. Using platinum (Pt) foil as the working electrode (anode), nickel (Ni) foam, and Ag/AgCl (3.0 M KCl) as the counter electrode and reference electrode, respectively, the authors tested their idea in a flow-cell setup with 1.0 M potassium chloride (KCl) electrolyte, in which they mixed the catholyte and anolyte output streams as displayed in Fig. 11b. Briefly, Cl^- is oxidized to Cl_2 at the Pt anode, which bonds with H_2O to form hypochlorous and hydrochloric acid (HOCl and HCl, respectively). HOCl then reacted with ethylene dissolved in the electrolyte to form ethylene chlorohydrin ($HOCH_2CH_2Cl$). Upon mixture of hydroxide (OH^-, from the catholyte stream) and $HOCH_2CH_2Cl$ (anolyte stream), ethylene oxide was generated, and Cl^- were regenerated. Through this modified system, they achieved a faradaic efficiency of ~70% and product specificities of ~97%.

Manthiram *et al.* conducted a series of electrochemical kinetic studies to understand the mechanism of ethylene oxidation in saline water using cobalt oxide nanoparticle catalysts and chlorine as a redox mediator.[169] Fig. 11c illustrates the electrochemical cell set-up used under simulated seawater electrolyte. Ethylene gas was introduced through the porous carbon paper anode. Given that 2-choloroethanol is expected to be formed as a product in the chlorohydrin process, it was hypothesized that the chloride ions in the electrolyte are likely to be oxidized to active chlorine species (*i.e.*, Cl_2, HOCl, and OCl^-) at the anode surface, which act as a redox mediator to oxidize ethylene. Among the suspected chlorine species, molecular chlorine was determined as most active for oxidizing ethylene to 2-choloroethanol and further aging of the as-electrolyzed solution converted 2-choloroethanol into ethylene oxide. Generally, chlorine evolution reaction (CER) under neutral pH follows the Krishtalik mechanism where the second electron-transfer step is the rate-determining step, that forms the adsorbed Cl^+ species. The authors found that in the presence of ethylene, the resting state and rate-determining step (RDS) of the chlorine-mediated ethylene oxidation reaction are different from that of CER.[170,171] The group suggested a new pathway where adsorbed chlorine exist as a resting state and one electron oxidation occurs to generate Cl^+ species, followed by the chemical rate-determining step to produce Cl_2 (Fig. 11d).

3.3.2. Allylic oxidation. The allylic oxidation of olefins is a very common C–H activation process that provides access to enones, which exhibit versatile polar reactivity. This transformation is of particular interest in the synthesis of natural products, pharmaceuticals, and flavor compounds.[172,173] In general, the most effective catalysts for allylic oxidation are those metals that readily go through 1-electron redox processes, *i.e.*, $Fe^{2+} \leftrightharpoons Fe^{3+}$, $Cu^{1+} \leftrightharpoons Cu^{2+}$, and $Co^{2+} \leftrightharpoons Co^{3+}$. Bearing this in mind, Doyle *et al.* developed a novel catalytic allylic oxidation protocol based on dirhodium(II) caprolactamate (denoted as $Rh_2(cap)_4$).[174] The unique reactivity of $Rh_2(cap)_4$ emanates from its ability to undergo facile redox chemistry, namely Rh_2^{4+}/Rh_2^{5+}. A minimum catalyst loading of 0.1 mol% $Rh_2(cap)_4$ was able to produce enedieones with impressive yield in just 1 h (Table 5, entries 3–8). However, toxic oxidizers and large solvent quantities are required for allylic oxidation *via* organic synthesis, which limits their application.

Consequently, electrochemistry was introduced to allylic oxidation to realize a robust, easy to use, and scalable electro-organic process. Masui *et al.* were the first to conduct anodic oxidation of olefins to α, β unsaturated ketones using *N*-hydroxyphthalimide (NHPI) as a redox mediator and atmospheric oxygen as an oxygen source.[175] However, unsatisfactory yield and selectivity were obtained and there was a limited scope in terms of accessible substrates. In response, Baran *et al.* improved the original scheme by employing a tetrachloro-derivative to enhance the reactivity of NHPI and *tert*-butylhydroperoxide (^{t}BuOOH) as co-oxidant (Fig. 12a).[176] They then proposed an optimized mechanism for electrochemical allylic oxidation using the modified mediator (Cl_4NHPI), as displayed in Fig. 12b. Briefly, the transformation of olefinic substrate **1** initially involves the deprotonation of Cl_4NHPI in the presence of excess pyridine, followed by the anodic oxidation, which generated tetra-chlorophthalimido *N*-oxyl radical species. Subsequently, olefin **1** proceeded to hydrogen atom abstraction, which induced the regeneration of the redox mediator and formation of allylic radical species **2**. Finally, the reaction between the radical species and electrochemically generated ^{t}BuOO$^\bullet$ produced allylic peroxide **3**, which, upon the removal of ^{t}BuOH, yielded enone **4**. Notably, the optimized method was successfully applied to more than 30 substrates with good yield and selectivity, thus demonstrating its practical utility.

3.3.3. Dihydroxylation reaction. Similar to epoxides and ketones, ethylene glycols are important precursors in the manufacture of polymers and anti-freeze formulation. Currently, large-scale synthesis of ethylene glycol from ethylene follows a two-step process *via* an oxirane intermediate, which generates a massive amount of CO_2. The cost of equipment and emission of CO_2 during the production of this compound might

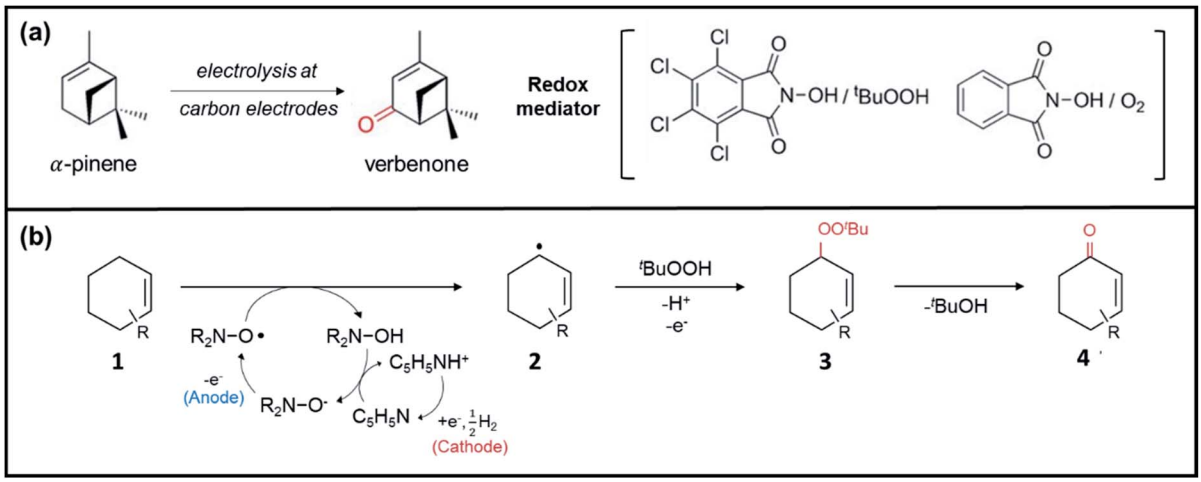

Fig. 12 (a) Anodic oxidation of α-pinene using the original and modified NHPI redox mediator. Reproduced with permission.[173] Copyright 2020, American Chemical Society. (b) Proposed mechanism for electrochemical allylic oxidation of olefins using the modified NHPI redox mediator. Reproduced with permission.[176] Copyright 2016, Macmillan Publishers Limited.

be minimized *via* a direct selective electrooxidation of ethylene. In line with this, Sargent *et al.* reported electrochemical oxidation of ethylene to ethylene glycol using palladium catalyst at ambient temperature and pressure.[177] During cyclic voltammetry (CV) measurements, they observed an obvious catalyst activation as evidenced by the substantial changes in growth and shift of the reduction peak with time. The reduction peak characteristics were correlated to the reduction of PdO to metallic Pd and the reduction of surface hydroxyl intermediates, such as *OH. A reaction mechanism on the PdO surface was proposed through DFT calculations, wherein they identified the second OH addition to the $*C_2H_4OH$ intermediate (IV → V) as the rate-determining step in ethylene glycol formation due to the high energy change of 0.74 eV associated with this process (Fig. 13a). Au dopants were added to the Pd catalyst to modulate the OH binding energy for step IV → V and to prevent further oxygenation of ethylene glycol. Remarkably, an average of 80% faradic efficiency toward ethylene glycol, at a partial current density of 5.7 mA cm^{-2}, was attained with no significant loss of performance during 100 h of continuous operation.

3.3.4. Oxygen functionalization reaction accompanied by C–H activation. The progress of direct C–H functionalization has led to the development of environmentally-benign and economically attractive bond formations that significantly reduce the number of synthetic operations, as well as the amount of unwanted by-products generated during organic synthesis.[178–186] However, the majority of earlier C–H functionalizations rely on precious transition metal catalysts like palladium, platinum, rhodium, ruthenium, and iridium, which mostly require stoichiometric quantities of chemical reagents such as Ag^{I} and Cu^{II} salts as sacrificial oxidants. On the other hand, electrochemical C–H activation has been considered a more ideal strategy as it exploits electricity to replace those by-product-generating chemical reagents.

Particular examples to discuss are the recent works of Surendranath *et al.*, which tackled new electrochemical approaches for promoting rapid methane monofunctionalization.[187] Fig. 13b displays their proposed mechanism for electrochemical methane functionalization driven by $Pd_2^{III,III}$ intermediate species. Specifically, $Pd^{II}SO_4$ was electrooxidized in concentrated sulfuric acid to form the $Pd_2^{III,III}$ species, which then reacts with methane. The activation of methane by the electrogenerated Pd species proceeds with low activation barrier energy (25.9 ± 2.6 kcal mol^{-1}), generating methyl bisulfate (CH_3OSO_3H) and methanesulfonic acid (CH_3SO_3H) as methanol precursors. Both of these methanol precursors can be thermally and hydrolytically converted to methanol *via* faradaic and non-faradaic pathways (green and blue arrows in Fig. 13b), respectively, which significantly increases the electrical energy efficiency of the reaction while maintaining high rates of catalysis. Afterward, an electrochemical approach for continuous, steady-state methane to methanol conversion was established in the presence of stoichiometric Pt^{IV} oxidants in Pt^{II} chloride salt aqueous solution ($Pt^{II}Cl_4^{2-}$) at a low reaction temperature (Fig. 13c).[188] They emphasized that, while the Cl-adsorbed Pt surfaces were active for the inner-sphere two-electron transfer of Pt^{II} to Pt^{IV}, this electrode is inert toward the simultaneous oxidation of methanol products. By careful optimization and maintenance of the Pt^{IV} : Pt^{II} ratio (4.3 : 1.4), it was possible to carry out steady-state and continuous methane to methane catalysis up to 30 h with 70% methanol selectivity.

Meanwhile, cobalt complexes have been recently identified as cost-effective electrochemical catalysts. Ackermann *et al.* reported for the first time the successful silver-free electrochemical cobalt-catalyzed C–H activation of arenes and alkenes *via* C–H oxygenation under mild conditions at 23 °C.[189] They identified $Co(OAc)_2$ as an optimal catalyst among a representative set of cobalt precursors, while NaOPiv showed better performance as a base than NaOAc. Also, control experiments showed that electrochemical C–H functionalization was not feasible without the presence of a base, electric current, and/or

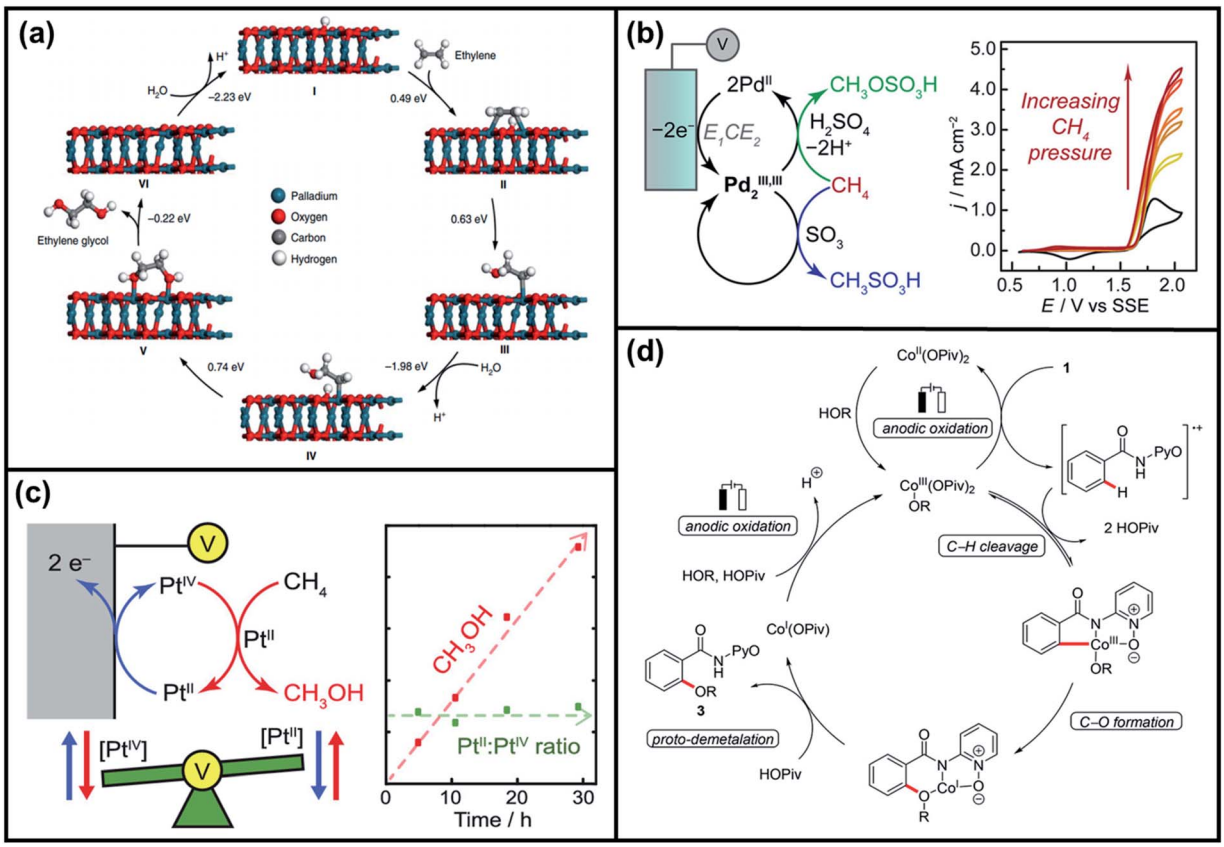

Fig. 13 (a) Proposed reaction mechanism of electrochemical oxidation of ethylene to ethylene glycols, in which DFT calculations implied the involvement of the lattice OH in PdO as a direct reaction intermediate. Reproduced with permission.[177] Copyright 2020, Springer Nature Limited. (b) Proposed mechanism for electrochemical methane functionalization by a $Pd_2^{III,III}$ intermediate. Green and blue arrows indicate faradaic and non-faradaic reaction pathways, respectively. Inset displays the methane functionalization by an electrogenerated $Pd_2^{III,III}$ species with varying CH_4 species. Reproduced with permission.[187] Copyright 2017, American Chemical Society. (c) Schematic of methane to methanol catalysis *via* the electrochemical regeneration of Pt^{IV}. Inset shows the effect of a constant Pt^{II} : Pt^{IV} ratio to methanol production with respect to reaction time. Reproduced with permission.[188] Copyright 2019, American Chemical Society. (d) Proposed catalytic cycle for electrochemical cobalt-catalyzed C–H oxygenation at room temperature. Reproduced with permission.[189] Copyright 2017, American Chemical Society.

cobalt catalyst. On the basis of their mechanistic studies, they proposed a catalytic cycle of the cobalt-catalyzed C–H activation. Fig. 13d shows that the reaction mechanism is possibly initiated by a facile electrochemical catalyst generation, followed by electrochemical single electron transfer of the aromatic benzamide *via* anodic oxidation. Subsequently, C–O bond formation occurs by chelation assistance, securing excellent positional selectivity. Then, the desired product is released while the catalytically active Co^{III} species is regenerated by means of anodic oxidation.

3.4. Overview of electrochemical oxygen functionalization

In section 3, we have discussed the great potential of electrochemical methods towards oxygen functionalization reactions in terms of (1) electro-oxidation pathways and (2) synthetic strategies. The first part of this section presented the growth of electrochemical method based on the electron transfer mechanisms, namely, direct electro-oxidation *via* outer-sphere electron transfer, indirect electro-oxidation with mediators, and direct electro-oxidation *via* inner-sphere electron transfer. Subsequently, we assessed the progress of this advanced method by presenting various electrically driven chemical-organic syntheses, in which we discussed the advancement of well-known electrochemical systems and catalyst designs. Fig. 14 represents the different types of electrochemical oxygen functionalization reactions discussed in this review.

As already stated, electrochemical methods can proceed with various oxygen functionalization reactions under milder conditions and with total elimination of unwanted by-products. More importantly, the exploitation of electricity as sole oxidant to drive the oxidation reactions has prevented the excessive use of harmful and toxic chemical oxidants, leading to a greener chemistry. However, the major obstacle for the commercialization of electro-organic synthesis is the required high energy cost correlated to the high overpotentials. The poor selectivity towards desired products and the difficulty to identify the suitable conditions under which the reaction could proceed selectively with high yield also raise a major obstruction for the proposed electrochemical approach. In addition, supporting electrolytes and additives are mostly required to reduce the

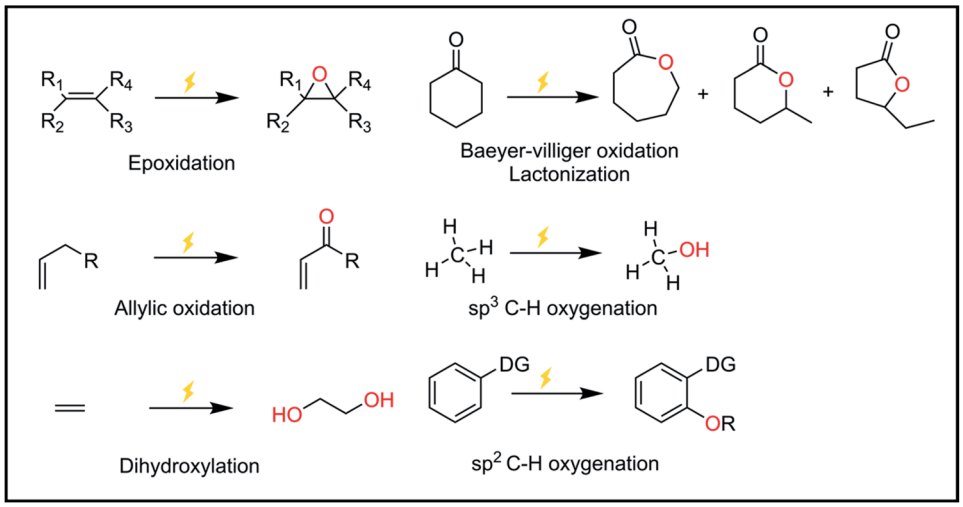

Fig. 14 Summary of previously studied electrochemical oxygen functionalization reactions.

ohmic resistance inflicted by the poor conductivity of organic solvents, which also poses a challenge in scaling up.

Because of the above-mentioned difficulties, immense efforts have been made to expand the application of electro-organic synthesis. For example, the use of water as an oxygen atom source is difficult (thermochemically), as it requires unreasonably high temperatures and pressures. However, the idea to apply an electrical potential instead of pressure, to release the oxygen from water and to eventually drive the chemical reaction between water and the olefin substrate, made it possible to use water as an oxygen atom source without any strong chemical oxidants. Significantly, the epoxidation of ethylene with water proceeded under room temperature and ambient pressure without the production of carbon dioxide or carbon monoxide. In this regard, we believe that electrochemical oxygen functionalization utilizing water can become an alternative methodology for the decarbonization of the chemical industry. Additionally, continuous efforts are given to the modification of the structure and composition of various electrocatalysts, search of suitable reaction media (solvent, additives, supporting electrolytes), and enhancement of the different electrochemical systems to fully optimize the overall performance of electrochemical oxygen functionalization in terms of selectivity, conversion, faradaic efficiency, and yield.

4. Summary and outlook

This Review article collectively highlights the recent development of oxygen functionalization reactions based on non-electrochemical and electrochemical methods. While the non-electrochemical methods may be considered as the conventional approach for the oxidation of organic substrates, the electrochemical process offers a greener chemistry as it can proceed the oxidation reaction under milder conditions with zero waste/unwanted by-products. However, the tangible progress of the latter progress is just beginning to blossom even though it has been studied for several decades. Hence, in the last part of this review, we hope to briefly discuss the future directions of electrochemistry towards the transformation of organic substrates into useful end products.

Various strategies have been exploited in an attempt to achieve selective electrochemical oxygen functionalization, but further breakthroughs must be made to realize its commercialization. To fully improve the performance of this innovative approach, it is imperative to understand the interfacial kinetics at the electrode. Oxidation at the anode always competes with other side reactions, such as oxygen evolution, solvent oxidation, oxidation of auxiliary functional groups, *etc.* Thus, we categorized the electrochemical methods with respect to their mechanisms: indirect electro-oxidation with mediators and direct oxidation with inner or outer sphere electron transfer mechanism, respectively. Notably, indirect oxidation in presence of a mediator has provided an efficient strategy to selectively oxidize target substrates using the redox potential of the redox mediator. Since the redox potential of the mediator is typically sufficiently lower than that of the substrates, the direct oxidation of the substrate at the electrode is avoided.

Tuning the binding affinity of reactants toward the electrode (catalyst) surface has been previously regarded as a vital technique in the field of electrochemical water splitting, oxygen reduction reactions, and carbon dioxide. Also, it was verified that selectivity and overpotential values are largely affected by the types of catalysts on the electrode. However, most studied schemes, including the so-called volcano plot based on the Sabatier principle, present the oxygen functionalization *via* an outer-sphere pathway, which limits the role of catalysts. Because the electrode surface is polarized and an electric double layer is formed when an external voltage is applied, it became necessary to examine the solvation phenomena of reactant species in blended electrolytes in order to boost the interaction between electrode materials and reactant species. In line with this, a direct electro-oxidation reaction following an inner-sphere mechanism is considered as an alternative way of directing selectivity correlated to its capacity to control the

interfacial kinetics happening on the electrode surface. We introduced in Section 3 the recent attempts to conduct oxygen functionalization reactions with inner-sphere fashion. In particular, Manthiram *et al.* mediated direct bond formation *via* pre-activation of water molecules (M=O or M–OH) as an oxygen source.[162]

Relevant to the aforementioned issues, deeper studies of interfacial kinetics in the electrochemical system should be explored. Because polarized electrode surfaces normally disfavor non-polar organic reactants, covalent bonding between the electrode surface and reactant species is hardly formed. To overcome this, solvation of solvent and electrolyte molecules may play a key role in enhancing the solubility and facilitating the approach of the reactant species. Kamlet–Taft parameters are solvochromic properties that contain polarizability, hydrogen bond donating, and accepting abilities of solvent molecules.[190,191] It was first suggested by Taft and Kamlet and has been widely utilized to predict the effect of solvent molecules on reaction kinetics, such as catalytic hydrogenation and cross-coupling reactions. Considering most oxygen-atom functionalization requires hydrogen/proton transfer, it is expected that an appropriate choice of solvent molecules based on K–T parameters might enhance the reaction efficiency.[192] We believe that this review provides the valuable insights for transition metal-based oxygen functionalization catalysis.

Author contributions

K. J. conceptualized the paper. G. M. T., Y. P., K. L., and K. J. prepared the original draft of the manuscript. G. M. T., K. L., and K. J. reviewed and edited its contents. K. L. and K. J. supervised the work.

Conflicts of interest

There are no conflicts to declare.

Acknowledgements

G. M. T., Y. P., and K. L. were supported by National Research Foundation of Korea (NRF-2020R1A2B5B03002475 and NRF-2019R1A6A1A11044070), the Korea Basic Science Institute under the R&D program (Project No. C38530) supervised by the Ministry of Science, and the Hydrogen Energy Innovation Technology Development Program of the National Research Foundation of Korea funded by the Korean government (Ministry of Science and ICT (MSIT)) (No. NRF-2019M3E6A1064709). K. J. was supported by the National Research Foundation of Korea (NRF) grant funded by the Korea government (MSIT) (No. NRF-2021R1C1C1004264) and a Korea University Grant.

Notes and references

1 R. L. Lieberman and A. C. Rosenzweig, *Crit. Rev. Biochem. Mol. Biol.*, 2004, **39**, 147–164.
2 J. C. Murreil, B. Gilbert and I. R. McDonald, *Arch. Microbiol.*, 2000, **173**, 325–332.
3 R. Banerjee, Y. Proshlyakov, J. D. Lipscomb and D. A. Proshlyakov, *Nature*, 2015, **518**, 431–434.
4 J. T. Groves, T. E. Nemo and R. S. Myers, *J. Am. Chem. Soc.*, 1979, **101**, 1032–1033.
5 J. T. Groves, *J. Chem. Educ.*, 1985, **62**, 924–927.
6 S. Fukuzumi, T. Kojima, Y. M. Lee and W. Nam, *Coord. Chem. Rev.*, 2017, **333**, 44–56.
7 V. A. Larson, B. Battistella, K. Ray, N. Lehnert and W. Nam, *Nat. Rev. Chem.*, 2020, **4**, 404–419.
8 I. Saikia, A. J. Borah and P. Phukan, *Chem. Rev.*, 2016, **116**, 6837–7042.
9 J. D. Lou and Z. N. Xu, *Tetrahedron Lett.*, 2002, **43**, 6095–6097.
10 C. Wang, L. Zong and C. H. Tan, *J. Am. Chem. Soc.*, 2015, **137**, 10677–10682.
11 J. Y. Li, Y. H. Li, M. Y. Qi, Q. Lin, Z. R. Tang and Y. J. Xu, *ACS Catal.*, 2020, **10**, 6262–6280.
12 C. Dai, J. Zhang, C. Huang and Z. Lei, *Chem. Rev.*, 2017, **117**, 6929–6983.
13 R. A. Sheldon, *J. Mol. Catal.*, 1983, **20**, 1–26.
14 Z. Guo, B. Liu, Q. Zhang, W. Deng, Y. Wang and Y. Yang, *Chem. Soc. Rev.*, 2014, **43**, 3480–3524.
15 R. H. Holm, *Chem. Rev.*, 1987, **87**, 1401–1449.
16 K. Weissermel and H.-J. Arpe, *Industrial Organic Chemistry*, WILEY-VCH, 4th edn, 2003, vol. 53.
17 Z. Shi, C. Zhang, C. Tang and N. Jiao, *Chem. Soc. Rev.*, 2012, **41**, 3381–3430.
18 S. Hu, W. Xiao, W. Yang, J. Yang, Y. Fang, J. Xiong, Z. Luo, H. Deng, Y. Guo, L. Zhang and J. Ding, *ACS Appl. Mater. Interfaces*, 2018, **10**, 17167–17174.
19 B. Yang and T. A. Manz, *RSC Adv.*, 2016, **6**, 88189–88215.
20 H. T. Li, Q. Gao, B. Han, Z. H. Ren, K. S. Xia and C. G. Zhou, *ACS Appl. Mater. Interfaces*, 2017, **9**, 371–380.
21 Y. Feng, J. England and L. Que, *ACS Catal.*, 2011, **1**, 1035–1042.
22 B. Wang, C. Li, K. Bin Cho, W. Nam and S. Shaik, *J. Chem. Theory Comput.*, 2013, **9**, 2519–2525.
23 K. P. Bryliakov, *Chem. Rev.*, 2017, **117**, 11406–11459.
24 M. Ciclosi, C. Dinoi, L. Gonsalvi, M. Peruzzini, E. Manoury and R. Poli, *Organometallics*, 2008, **27**, 2281–2286.
25 Y. Yi, L. Wang, G. Li and H. Guo, *Catal. Sci. Technol.*, 2016, **6**, 1593–1610.
26 S. P. Teong, X. Li and Y. Zhang, *Green Chem.*, 2019, **21**, 5753–5780.
27 D. W. Low, J. R. Winkler and H. B. Gray, *J. Am. Chem. Soc.*, 1996, **118**, 117–120.
28 Y. M. Lee, S. N. Dhuri, S. C. Sawant, J. Cho, M. Kubo, T. Ogura, S. Fukuzumi and W. Nam, *Angew. Chem., Int. Ed.*, 2009, **48**, 1803–1806.
29 M. D. Kärkäs and B. Åkermark, *Dalton Trans.*, 2016, **45**, 14421–14461.
30 S. Fukuzumi, T. Kishi, H. Kotani, Y. M. Lee and W. Nam, *Nat. Chem.*, 2011, **3**, 38–41.
31 D. Shen, C. Saracini, Y. M. Lee, W. Sun, S. Fukuzumi and W. Nam, *J. Am. Chem. Soc.*, 2016, **138**, 15857–15860.

32 X. Engelmann, I. Monte-Pérez and K. Ray, *Angew. Chem., Int. Ed.*, 2016, **55**, 7632–7649.
33 M. Guo, T. Corona, K. Ray and W. Nam, *ACS Cent. Sci.*, 2019, **5**, 13–28.
34 S. Sahu and D. P. Goldberg, *J. Am. Chem. Soc.*, 2016, **138**, 11410–11428.
35 K. Ray, F. F. Pfaff, B. Wang and W. Nam, *J. Am. Chem. Soc.*, 2014, **136**, 13942–13958.
36 Z. Chen and G. Yin, *Chem. Soc. Rev.*, 2015, **44**, 1083–1100.
37 E. P. Talsi and K. P. Bryliakov, *Coord. Chem. Rev.*, 2012, **256**, 1418–1434.
38 K. P. Bryliakov and E. P. Talsi, *Coord. Chem. Rev.*, 2014, **276**, 73–96.
39 R. V. Ottenbacher, E. P. Talsi and K. P. Bryliakov, *Molecules*, 2016, **21**, 1454–1470.
40 A. Bassan, M. R. A. Blomberg, T. Borowski and P. E. M. Siegbahn, *J. Phys. Chem. B*, 2004, **108**, 13031–13041.
41 M. M. Abu-Omar, A. Loaiza and N. Hontzeas, *Chem. Rev.*, 2005, **105**, 2227–2252.
42 K. Chen, M. Costas and L. Que, *Dalton Trans.*, 2002, 672–679.
43 J. T. Groves, R. C. Haushalter, M. Nakamura, T. E. Nemo and B. J. Evans, *J. Am. Chem. Soc.*, 1981, **103**, 2884–2886.
44 J. T. Groves and Y. Watanabe, *J. Am. Chem. Soc.*, 1988, **110**, 8443–8452.
45 R. Andreu, E. E. Ferapontova, L. Gorton and J. J. Calvente, *J. Phys. Chem. B*, 2007, **111**, 469–477.
46 M. B. Neibergall, A. Stubna, Y. Mekmouche, E. Münck and J. D. Lipscomb, *Biochemistry*, 2007, **46**, 8004–8016.
47 J. T. Groves, J. Lee and S. S. Marla, *J. Am. Chem. Soc.*, 1997, **119**, 6269–6273.
48 J. Yano and V. Yachandra, *Chem. Rev.*, 2014, **114**, 4175–4205.
49 K. J. Young, B. J. Brennan, R. Tagore and G. W. Brudvig, *Acc. Chem. Res.*, 2015, **48**, 567–574.
50 X. X. Li, M. Guo, B. Qiu, K. Bin Cho, W. Sun and W. Nam, *Inorg. Chem.*, 2019, **58**, 14842–14852.
51 F. Teixeira, R. A. Mosquera, A. Melo, C. Freire and M. N. D. S. Cordeiro, *Phys. Chem. Chem. Phys.*, 2014, **16**, 25364–25376.
52 E. M. McGarrigle and D. G. Gilheany, *Chromium— and Manganese—Salen Promoted Epoxidation of Alkenes*, 2005, vol. 36.
53 N. Kannan, A. R. Patil and A. Sinha, *Dalton Trans.*, 2020, **49**, 14344–14360.
54 T. Ishizuka, H. Kotani and T. Kojima, *Dalton Trans.*, 2016, **45**, 16727–16750.
55 Z. Lv, W. Zheng, Z. Chen, Z. Tang, W. Mo and G. Yin, *Dalton Trans.*, 2016, **45**, 11369–11383.
56 Y. Liu and T. C. Lau, *J. Am. Chem. Soc.*, 2019, **141**, 3755–3766.
57 J. T. Groves and R. Quinn, *Inorg. Chem.*, 1984, **23**, 3844–3846.
58 J. T. Groves and R. Quinn, *J. Am. Chem. Soc.*, 1985, **107**, 5790–5792.
59 F. Zaera, *J. Phys. Chem. B*, 2002, **106**, 4043–4052.
60 C. M. Friend and B. Xu, *Acc. Chem. Res.*, 2017, **50**, 517–521.
61 W. Nam, Y. M. Lee and S. Fukuzumi, *Acc. Chem. Res.*, 2014, **47**, 1146–1154.
62 C. C. Phifer and D. R. McMillin, *Inorg. Chem.*, 1986, **25**, 1329–1333.
63 W. Nam, S. Y. Oh, Y. J. Sun, J. Kim, W. K. Kim, S. K. Woo and W. Shin, *J. Org. Chem.*, 2003, **68**, 7903–7906.
64 C. M. Elliott, J. R. Dunkle and S. C. Paulson, *Langmuir*, 2005, **21**, 8605–8608.
65 T. Niwa and M. Nakada, *J. Am. Chem. Soc.*, 2012, **134**, 13538–13541.
66 B. Mondal, F. Neese, E. Bill and S. Ye, *J. Am. Chem. Soc.*, 2018, **140**, 9531–9544.
67 K. K. Singh, M. K. Tiwari, B. B. Dhar, K. Vanka and S. Sen Gupta, *Inorg. Chem.*, 2015, **54**, 6112–6121.
68 C. Krebs, D. G. Fujimori, C. T. Walsh and J. M. Bollinger, *Acc. Chem. Res.*, 2007, **40**, 484–492.
69 H. Miyake, K. Chen, S. J. Lange and L. Que, *Inorg. Chem.*, 2001, **40**, 3534–3538.
70 M. A. Ehudin, L. B. Gee, S. Sabuncu, A. Braun, P. Moënne-Loccoz, B. Hedman, K. O. Hodgson, E. I. Solomon and K. D. Karlin, *J. Am. Chem. Soc.*, 2019, **141**, 5942–5960.
71 M. J. Park, J. Lee, Y. Sun, J. Kim and W. Nam, *J. Am. Chem. Soc.*, 2006, **128**, 2630–2634.
72 J. Serrano-Plana, A. Aguinaco, R. Belda, E. García-España, M. G. Basallote, A. Company and M. Costas, *Angew. Chem.*, 2016, **128**, 6418–6422.
73 J. R. Lindsay Smith and G. B. Shul'pin, *Tetrahedron Lett.*, 1998, **39**, 4909–4912.
74 C. Choe, L. Yang, Z. Lv, W. Mo, Z. Chen, G. Li and G. Yin, *Dalton Trans.*, 2015, **44**, 9182–9192.
75 G. B. Shul'pin, G. Süss-Fink and L. S. Shul'pina, *J. Mol. Catal. A: Chem.*, 2001, **170**, 17–34.
76 J. Du, C. Miao, C. Xia, Y. M. Lee, W. Nam and W. Sun, *ACS Catal.*, 2018, **8**, 4528–4538.
77 R. Zong and R. P. Thummel, *J. Am. Chem. Soc.*, 2005, **127**, 12802–12803.
78 G. A. Barf and R. A. Sheldon, *J. Mol. Catal. A*, 1995, **98**, 143–146.
79 J. L. Zhang, H. B. Zhou, J. S. Huang and C. M. Che, *Chem.–Eur. J.*, 2002, **8**, 1554–1562.
80 B. Chandra, K. K. Singh and S. Sen Gupta, *Chem. Sci.*, 2017, **8**, 7545–7551.
81 T. Shiragami, K. Kubomura, D. Ishibashi and H. Inoue, *J. Am. Chem. Soc.*, 1996, **118**, 6311–6312.
82 S. Funyu, T. Isobe, S. Takagi, D. A. Tryk and H. Inoue, *J. Am. Chem. Soc.*, 2003, **125**, 5734–5740.
83 K. Kurimoto, T. Yamazaki, Y. Suzuri, Y. Nabetani, S. Onuki, S. Takagi, T. Shimada, H. Tachibana and H. Inoue, *Photochem. Photobiol. Sci.*, 2014, **13**, 154–156.
84 D. Tatsumi, T. Tsukamoto, R. Honna, S. Hoshino, T. Shimada and S. Takagi, *Chem. Lett.*, 2017, **46**, 1311–1314.
85 J. W. Han, J. Jung, Y. M. Lee, W. Nam and S. Fukuzumi, *Chem. Sci.*, 2017, **8**, 7119–7125.
86 W. Huang, G. Sun and T. Cao, *Chem. Soc. Rev.*, 2017, **46**, 1977–2000.
87 T. Pu, H. Tian, M. E. Ford, S. Rangarajan and I. E. Wachs, *ACS Catal.*, 2019, 10727–10750.

88 T. E. Jones, R. Wyrwich, S. Böcklein, E. A. Carbonio, M. T. Greiner, A. Y. Klyushin, W. Moritz, A. Locatelli, T. O. Menteş, M. A. Niño, A. Knop-Gericke, R. Schlögl, S. Günther, J. Wintterlin and S. Piccinin, *ACS Catal.*, 2018, **8**, 3844–3852.
89 K. Weissermel and H.-J. Arpe, *Industrial Organic Chemistry*, Weinheim, New York, 1993.
90 A. J. F. Van Hoof, E. A. R. Hermans, A. P. Van Bavel, H. Friedrich and E. J. M. Hensen, *ACS Catal.*, 2019, **9**, 9829–9839.
91 S. Anandhakumar, M. Sasidharan, C. W. Tsao and A. M. Raichur, *ACS Appl. Mater. Interfaces*, 2014, **6**, 3275–3281.
92 S. S. Sangaru, H. Zhu, D. C. Rosenfeld, A. K. Samal, D. Anjum and J. M. Basset, *ACS Appl. Mater. Interfaces*, 2015, **7**, 28568–28576.
93 N. L. Nguyen, S. Piccinin and S. De Gironcoli, *J. Phys. Chem. C*, 2011, **115**, 10073–10079.
94 P. Christopher and S. Linic, *J. Am. Chem. Soc.*, 2008, **130**, 11264–11265.
95 P. Christopher and S. Linic, *ChemCatChem*, 2010, **2**, 78–83.
96 S. Linic and P. Christopher, *ChemCatChem*, 2010, **2**, 1061–1063.
97 M. Huš and A. Hellman, *ACS Catal.*, 2019, **9**, 1183–1196.
98 T. E. Jones, R. Wyrwich, S. Bocklein, T. C. R. Rocha, E. A. Carbonio, A. Knop-Gericke, R. Schlogl, S. Gunther, J. Wintterlin and S. Piccinin, *J. Phys. Chem. C*, 2016, **120**, 28630–28638.
99 C. S. Martín, *J. Chem. Eng. Data*, 2001, **46**, 1149–1152.
100 M. Drache, P. Roussel and J. P. Wignacourt, *Chem. Rev.*, 2007, **107**, 80–96.
101 C. Noguez, *J. Phys. Chem. C*, 2007, **111**, 3606–3619.
102 C. Liu, J. Xin, J. Tan, T. Liu, M. R. Kessler and J. Zhang, *ACS Omega*, 2018, **3**, 8718–8723.
103 H. Mimoun, M. Mignard, P. Brechot and L. Saussine, *J. Am. Chem. Soc.*, 1986, **108**, 3711–3718.
104 M. G. Clerici, G. Bellussi and U. Romano, *J. Catal.*, 1991, **129**, 159–167.
105 M. G. Clerici and P. Ingallina, *J. Catal.*, 1993, **140**, 71–83.
106 T. A. Nijhuis, M. Makkee, J. A. Moulijn and B. M. Weckhuysen, *Ind. Eng. Chem. Res.*, 2006, **45**, 3447–3459.
107 J. Teržan, M. Huš, B. Likozar and P. Djinović, *ACS Catal.*, 2020, 13415–13436.
108 T. Hayashi, K. Tanaka and M. Haruta, *J. Catal.*, 1998, **178**, 566–575.
109 B. S. Uphade, Y. Yamada, T. Akita, T. Nakamura and M. Haruta, *Appl. Catal., A*, 2001, **215**, 137–148.
110 B. S. Uphade, T. Akita, T. Nakamura and M. Haruta, *J. Catal.*, 2002, **209**, 331–340.
111 G. J. Hutchings, *J. Catal.*, 1985, **96**, 292–295.
112 M. Haruta, N. Yamada, T. Kobayashi and S. Iijima, *J. Catal.*, 1989, **115**, 301–309.
113 J. Gaudet, K. K. Bando, Z. Song, T. Fujitani, W. Zhang, D. S. Su and S. T. Oyama, *J. Catal.*, 2011, **280**, 40–49.
114 B. Gómez, N. V. Likhanova, M. A. Domínguez-Aguilar, R. Martínez-Palou, A. Vela and J. L. Gázquez, *J. Phys. Chem. B*, 2006, **110**, 8928–8934.
115 D. M. Perez Ferrandez, I. Herguedas Fernandez, M. P. G. Teley, M. H. J. M. De Croon, J. C. Schouten and T. A. Nijhuis, *J. Catal.*, 2015, **330**, 396–405.
116 X. Feng, N. Sheng, Y. Liu, X. Chen, D. Chen, C. Yang and X. Zhou, *ACS Catal.*, 2017, **7**, 2668–2675.
117 M. Haruta, B. S. Uphade, S. Tsubota and A. Miyamoto, *Res. Chem. Intermed.*, 1998, **24**, 329–336.
118 J. C. Liu, Y. Tang, C. R. Chang, Y. G. Wang and J. Li, *ACS Catal.*, 2016, **6**, 2525–2535.
119 S. Biella and M. Rossi, *Chem. Commun.*, 2003, **3**, 378–379.
120 S. Bang, Y. M. Lee, S. Hong, K. Bin Cho, Y. Nishida, M. S. Seo, R. Sarangi, S. Fukuzumi and W. Nam, *Nat. Chem.*, 2014, **6**, 934–940.
121 E. Y. Tsui, R. Tran, J. Yano and T. Agapie, *Nat. Chem.*, 2013, **5**, 293–299.
122 J. S. Kanady, E. Y. Tsui, M. W. Day and T. Agapie, *Science*, 2013, **333**, 733–737.
123 M. Yan, Y. Kawamata and P. S. Baran, *Chem. Rev.*, 2017, **117**, 13230–13319.
124 R. Francke and R. D. Little, *Chem. Soc. Rev.*, 2014, **43**, 2492–2521.
125 F. Wang and S. S. Stahl, *Acc. Chem. Res.*, 2020, **53**, 561–574.
126 D. T. Mah, *Electrochem. Soc. Interface*, 2014, **23**, 47.
127 J. H. Wagenknecht, *J. Chem. Educ.*, 1983, **60**, 271–273.
128 L. M. Torres, A. F. Gil, L. Galicia and I. González, *J. Chem. Educ.*, 1996, **73**, 808–810.
129 A. J. Bard, *J. Am. Chem. Soc.*, 2010, **132**, 7559–7567.
130 S. Tanimoto and A. Ichimura, *J. Chem. Educ.*, 2013, **90**, 778–781.
131 N. Elgrishi, K. J. Rountree, B. D. McCarthy, E. S. Rountree, T. T. Eisenhart and J. L. Dempsey, *J. Chem. Educ.*, 2018, **95**, 197–206.
132 S. J. Hendel and E. R. Young, *J. Chem. Educ.*, 2016, **93**, 1951–1956.
133 I. Landa-Medrano, I. Lozano, N. Ortiz-Vitoriano, I. Ruiz De Larramendi and T. Rojo, *J. Mater. Chem. A*, 2019, **7**, 8746–8764.
134 G. S. Sauer and S. Lin, *ACS Catal.*, 2018, **8**, 5175–5187.
135 N. T. Zhang, C. C. Zeng, C. M. Lam, R. K. Gbur and R. D. Little, *J. Org. Chem.*, 2013, **78**, 2104–2110.
136 P. Cao, Y. Sun, J. Yao, B. Ren, R. Gu and Z. Tian, *Langmuir*, 2002, **18**, 2737–2742.
137 I. Streeter, A. J. Wain, M. Thompson and R. G. Compton, *J. Phys. Chem. B*, 2005, **109**, 12636–12649.
138 G. V. Ramesh, R. Kodiyath, T. Tanabe, M. Manikandan, T. Fujita, N. Umezawa, S. Ueda, S. Ishihara, K. Ariga and H. Abe, *ACS Appl. Mater. Interfaces*, 2014, **6**, 16124–16130.
139 J. Wu, Y. Zhou, Y. Zhou, C. W. Chiang and A. Lei, *ACS Catal.*, 2017, **7**, 8320–8323.
140 J. W. Lee, J. Y. Shin, Y. S. Chun, H. Bin Jang, C. E. Song and S. G. Lee, *Acc. Chem. Res.*, 2010, **43**, 985–994.
141 I. A. Ansari and R. Gree, *Org. Lett.*, 2002, **4**, 1507–1509.
142 W. Zheng, M. Wu, C. Yang, Y. Chen, R. Tan and D. Yin, *Mater. Chem. Phys.*, 2020, **256**, 123681.

143 J. Ghilane, P. Martin, H. Randriamahazaka and J. C. Lacroix, *Electrochem. Commun.*, 2010, **12**, 246–249.
144 Y. L. Hu, Q. F. Liu, T. T. Lu and M. Lu, *Catal. Commun.*, 2010, **11**, 923–927.
145 M. Kathiresan and D. Velayutham, *Chem. Commun.*, 2015, **51**, 17499–17516.
146 G. Zhao, T. Jiang, W. Wu, B. Han, Z. Liu and H. Gao, *J. Phys. Chem. B*, 2004, **108**, 13052–13057.
147 C. Margarita and H. Lundberg, *Catalysts*, 2020, **10**, 1–24.
148 M. Panizza and G. Cerisola, *Chem. Rev.*, 2009, **109**, 6541–6569.
149 J. B. Sperr and D. L. Wright, *Chem. Soc. Rev.*, 2006, **35**, 605–621.
150 C. Yu, B. Özkaya and F. W. Patureau, *Chem.–Eur. J.*, 2021, **27**, 3682–3687.
151 Y. Imada, Y. Okada, K. Noguchi and K. Chiba, *Angew. Chem., Int. Ed.*, 2019, **58**, 125–129.
152 K. Liu, C. Song and A. Lei, *Org. Biomol. Chem.*, 2018, **16**, 2375–2387.
153 H. T. Tang, J. S. Jia and Y. M. Pan, *Org. Biomol. Chem.*, 2020, **18**, 5315–5333.
154 R. Lin, A. P. Amrute and J. Pérez-Ramírez, *Chem. Rev.*, 2017, **117**, 4182–4247.
155 S. Torii, K. Uneyama, H. Tanaka, T. Yamanaka, T. Yasuda, M. Ono and Y. Kohmoto, *J. Org. Chem.*, 1981, **46**, 3312–3315.
156 S. Torii, P. Liu, N. Bhuvaneswari, C. Amatore and A. Jutand, *J. Org. Chem.*, 1996, **61**, 3056–3060.
157 H. Tanaka, M. Kuroboshi, H. Takeda, H. Kanda and S. Torii, *J. Electroanal. Chem.*, 2001, **507**, 75–81.
158 H. Nishihara, K. Pressprich, R. W. Murray and J. P. Coliman, *Inorg. Chem.*, 1990, **29**, 1000–1006.
159 L. Espinal, S. L. Suib and J. F. Rusling, *J. Am. Chem. Soc.*, 2004, **126**, 7676–7682.
160 K. P. Ho, K. Y. Wong and T. H. Chan, *Tetrahedron*, 2006, **62**, 6650–6658.
161 Z. J. Schiffer and K. Manthiram, *Joule*, 2017, **1**, 10–14.
162 K. Jin, J. H. Maalouf, N. Lazouski, N. Corbin, D. Yang and K. Manthiram, *J. Am. Chem. Soc.*, 2019, **141**, 6413–6418.
163 J. H. Maalouf, K. Jin, D. Yang, A. M. Limaye and K. Manthiram, *ACS Catal.*, 2020, **10**, 5750–5756.
164 J. M. Van der Eijk, T. H. Peters, N. De Wit and H. A. Colijn, *Catal. Today*, 1988, **3**, 259–266.
165 C. G. Vayenas, S. Bebelis and S. Neophytides, *J. Phys. Chem.*, 1988, **92**, 5083–5085.
166 S. Bebelis and C. G. Vayenas, *J. Catal.*, 1992, **138**, 588–610.
167 J. S. Jirkovský, M. Busch, E. Ahlberg, I. Panas and P. Krtil, *J. Am. Chem. Soc.*, 2011, **133**, 5882–5892.
168 W. R. Leow, Y. Lum, A. Ozden, Y. Wang, D. H. Nam, B. Chen, J. Wicks, T. T. Zhuang, F. Li, D. Sinton and E. H. Sargent, *Science*, 2020, **368**, 1228–1233.
169 M. Chung, K. Jin, J. S. Zeng and K. Manthiram, *ACS Catal.*, 2020, 14015–14023.
170 L. I. Krishtalik, *Electrochim. Acta*, 1981, **26**, 329–337.
171 H. Ha, K. Jin, S. Park, K. G. Lee, K. H. Cho, H. Seo, H. Y. Ahn, Y. H. Lee and K. T. Nam, *J. Phys. Chem. Lett.*, 2019, **10**, 1226–1233.
172 W. G. Dauben, M. Lorber and D. S. Fullerton, *J. Org. Chem.*, 1969, **34**, 3587–3592.
173 S. R. Waldvogel and M. Selt, *Angew. Chem., Int. Ed.*, 2016, **55**, 12578–12580.
174 A. J. Catino, R. E. Forslund and M. P. Doyle, *J. Am. Chem. Soc.*, 2004, **126**, 13622–13623.
175 M. Masui, S. Hara, T. Ueshima, T. Kawaguchi and S. Ozaki, *Chem. Pharm. Bull.*, 1983, **31**, 4209–4211.
176 E. J. Horn, B. R. Rosen, Y. Chen, J. Tang, K. Chen, M. D. Eastgate and P. S. Baran, *Nature*, 2016, **533**, 77–81.
177 Y. Lum, J. E. Huang, Z. Wang, M. Luo, D. H. Nam, W. R. Leow, B. Chen, J. Wicks, Y. C. Li, Y. Wang, C. T. Dinh, J. Li, T. T. Zhuang, F. Li, T. K. Sham, D. Sinton and E. H. Sargent, *Nat. Catal.*, 2020, **3**, 14–22.
178 M. D. Kärkäs, *Chem. Soc. Rev.*, 2018, **47**, 5786–5865.
179 M. Moselage, J. Li and L. Ackermann, *ACS Catal.*, 2016, **6**, 498–525.
180 N. Sauermann, T. H. Meyer, Y. Qiu and L. Ackermann, *ACS Catal.*, 2018, **8**, 7086–7103.
181 K. Ogura and K. Takamagari, *Nature*, 1986, **319**, 308.
182 M. Ma, B. J. Jin, P. Li, M. S. Jung, J. Il Kim, Y. Cho, S. Kim, J. H. Moon and J. H. Park, *Adv. Sci.*, 2017, **4**, 1700379.
183 L. Arnarson, P. S. Schmidt, M. Pandey, A. Bagger, K. S. Thygesen, I. E. L. Stephens and J. Rossmeisl, *Phys. Chem. Chem. Phys.*, 2018, **20**, 11152–11159.
184 Y. Kawamata, M. Yan, Z. Liu, D. H. Bao, J. Chen, J. T. Starr and P. S. Baran, *J. Am. Chem. Soc.*, 2017, **139**, 7448–7451.
185 M. J. Boyd, A. A. Latimer, C. F. Dickens, A. C. Nielander, C. Hahn, J. K. Nrskov, D. C. Higgins and T. F. Jaramillo, *ACS Catal.*, 2019, **9**, 7578–7587.
186 M. Stoukides, *J. Appl. Electrochem.*, 1995, **25**, 899–912.
187 M. E. O'Reilly, R. S. Kim, S. Oh and Y. Surendranath, *ACS Cent. Sci.*, 2017, **3**, 1174–1179.
188 R. S. Kim and Y. Surendranath, *ACS Cent. Sci.*, 2019, **5**, 1179–1186.
189 N. Sauermann, T. H. Meyer, C. Tian and L. Ackermann, *J. Am. Chem. Soc.*, 2017, **139**, 18452–18455.
190 R. W. Taft and M. J. Kamlet, *J. Am. Chem. Soc.*, 1976, **98**, 2886–2894.
191 M. J. Kamlet, J. L. M. Abboud, M. H. Abraham and R. W. Taft, *J. Org. Chem.*, 1983, **48**, 2877–2887.
192 L. Crowhurst, R. Falcone, N. L. Lancaster, V. Llopis-Mestre and T. Welton, *J. Org. Chem.*, 2006, **71**, 8847–8853.
193 W. Nam, *Acc. Chem. Res.*, 2007, **40**, 522–531.
194 S. Kim, K. Bin Cho, Y. M. Lee, J. Chen, S. Fukuzumi and W. Nam, *J. Am. Chem. Soc.*, 2016, **138**, 10654–10663.